LEVEL II

SDAC-TR-77-3

12

AD A066325

DDC FILE COPY

STUDY OF SELECTED EVENTS IN THE PAMIRS IN A SEISMIC DISCRIMINATION CONTEXT

P.A. SOBEL, D.H. VON SEGGERN, E.I. SWEETSER & D.W. RIVERS

Seismic Data Analysis Center

Teledyne Geotech, 314 Montgomery Street, Alexandria, Virginia 22314

10 OCTOBER 1977

APPROVED FOR PUBLIC RELEASE; DISTRIBUTION UNLIMITED.

Sponsored by

The Defense Advanced Research Projects Agency (DARPA)

ARPA Order No. 2551

Monitored By

AFTAC/VSC

312 Montgomery Street, Alexandria, Virginia 22314

DDC
RECEIVED
MAR 26 1979
D

79 03 22 064

Disclaimer: Neither the Defense Advanced Research Projects Agency nor the Air Force Technical Applications Center will be responsible for information contained herein which has been supplied by other organizations or contractors, and this document is subject to later revision as may be necessary. The views and conclusions presented are those of the authors and should not be interpreted as necessarily representing the official policies, either expressed or implied, of the Defense Advanced Research Projects Agency, the Air Force Technical Applications Center, or the US Government.

Unclassified

SECURITY CLASSIFICATION OF THIS PAGE (When Data Entered)

REPORT DOCUMENTATION PAGE

READ INSTRUCTIONS BEFORE COMPLETING FORM

1. REPORT NUMBER: 14 SDAC-TR-77-3

2. GOVT ACCESSION NO.

3. RECIPIENT'S CATALOG NUMBER

4. TITLE (and Subtitle): 16 STUDY OF SELECTED EVENTS IN THE PAMIRS IN A SEISMIC DISCRIMINATION CONTEXT.

5. TYPE OF REPORT & PERIOD COVERED: 9 Technical rept.

6. ~~PERFORMING ORG. REPORT NUMBER~~

7. AUTHOR(s): 10 P.A. Sobel, D.H. von Seggern, E.I. Sweetser, D.W. Rivers

8. CONTRACT OR GRANT NUMBER(s): 15 F08606-77-C-0014, ARPA Order-2551

9. PERFORMING ORGANIZATION NAME AND ADDRESS:
Teledyne Geotech
314 Montgomery Street
Alexandria, Virginia 22314

10. PROGRAM ELEMENT, PROJECT, TASK AREA & WORK UNIT NUMBERS: VT/7709

11. CONTROLLING OFFICE NAME AND ADDRESS:
Defense Advanced Research Projects Agency
Nuclear Monitoring Research Office
1400 Wilson Blvd, Arlington, Virginia 22209

12. REPORT DATE: 11 10 Oct~~ober 1977~~

13. NUMBER OF PAGES: 71

14. MONITORING AGENCY NAME & ADDRESS (if different from Controlling Office):
VELA Seismological Center
312 Montgomery Street
Alexandria, Virginia 22314

15. SECURITY CLASS. (of this report): Unclassified

15a. DECLASSIFICATION DOWNGRADING SCHEDULE

16. DISTRIBUTION STATEMENT (of this Report)

APPROVED FOR PUBLIC RELEASE; DISTRIBUTION UNLIMITED.

12 74p.

17. DISTRIBUTION STATEMENT (of the abstract entered in Block 20, if different from Report)

18. SUPPLEMENTARY NOTES

Author's Report Date 04/08/77

19. KEY WORDS (Continue on reverse side if necessary and identify by block number)

Pamirs
Seismic Discrimination
Underground Nuclear Explosions
M_s versus m_b

20. ABSTRACT (Continue on reverse side if necessary and identify by block number)

Eleven earthquakes with low reported M_s for their m_b from the Northern Pamirs were examined in a seismic discrimination context. Seismograms from ALPA, LASA, NORSAR, the HGLP and the WWSSN stations were studied for source mechanism, M_s-m_b, corner frequency, pP, complexity, and spectral ratio. All the Pamir events can be identified as earthquakes when their characteristics are compared to those of Kazakh explosions. P-waves to NORSAR from these earthquakes exhibit very high frequency, and their spectral corner frequencies are not distinctly different from those of explosions.

sub s sub b sub s

DD FORM 1 JAN 73 1473 EDITION OF 1 NOV 65 IS OBSOLETE

Unclassified

SECURITY CLASSIFICATION OF THIS PAGE (When Data Entered)

408 258

xlt

STUDY OF SELECTED EVENTS IN THE PAMIRS

IN A SEISMIC DISCRIMINATION CONTEXT

SEISMIC DATA ANALYSIS CENTER REPORT NO.: SDAC-TR-77-3

AFTAC Project Authorization No.:	VELA
Project Title:	Seismic Data Analysis Center
ARPA Order No.:	2551
ARPA Program Code No.:	7F10
Name of Contractor:	TELEDYNE GEOTECH
Contract No.:	F08606-77-C-0014
Date of Contract:	01 October 1976
Amount of Contract:	$3,005,183
Contract Expiration Date:	30 September 1977
Project Manager:	Robert R. Blandford (703) 836-3882

P. O. Box 334, Alexandria, Virginia 22314

APPROVED FOR PUBLIC RELEASE; DISTRIBUTION UNLIMITED.

ACCESSION for
NTIS White Section
DDC Buff Section
UNANNOUNCED
JUSTIFICATION
BY
DISTRIBUTION/AVAILABILITY CODES
Dist. AVAIL. and/or SPECIAL
A

DDC
RECEIVED
MAR 26 1979
D

79 03 22 064

ABSTRACT

Eleven earthquakes with low reported M_s for their m_b from the Northern Pamirs were examined in a seismic discrimination context. Seismograms from ALPA, LASA, NORSAR, the HGLP and the WWSSN stations were studied for source mechanism, M_s-m_b, corner frequency, pP, complexity, and spectral ratio. All the Pamir events can be identified as earthquakes when their characteristics are compared to those of Kazakh explosions. P-waves to NORSAR from these earthquakes exhibit very high frequency, and their spectral corner frequencies are not distinctly different from those of explosions.

TABLE OF CONTENTS

LIST OF FIGURES

LIST OF FIGURES (Continued)

LIST OF TABLES

INTRODUCTION

Discrimination parameters have been applied in detail at only a few nuclear test sites and earthquake regions. This study is part of a series which will extend these discrimination studies to other regions of shallow earthquakes. This particular report examines eleven earthquakes in the Northern Pamirs which had low reported M_s for their m_b, such that these events fall close to the explosion population on a M_s-m_b graph. Most of the earthquakes in the Pamirs are probably associated with large thrust faults, which are a result of the Indian-Eurasian collision. Actual seismogram analysis revealed that the events chosen were too small to determine their fault-plane solutions. Paramount in this study is the determination of average M_s and m_b for selected events. Further, we investigate other common discrimination parameters such as first motions, corner frequency, complexity, and short-period spectral ratios. Results for the Pamir events will be compared to Kazakh explosions and related to the available geophysical data on the crust and upper mantle of the region.

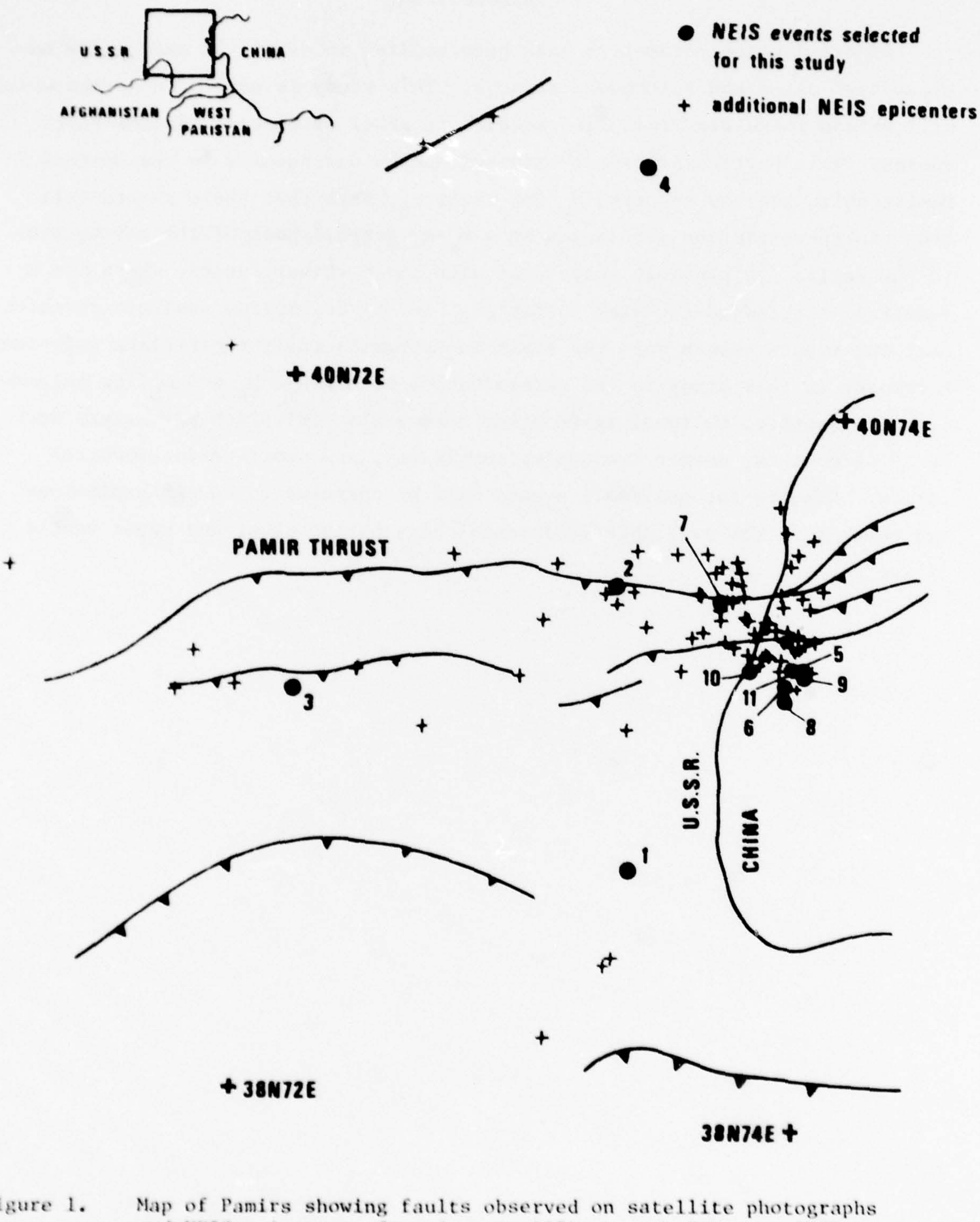

Figure 1. Map of Pamirs showing faults observed on satellite photographs and NEIS epicenters from January 1971 through February 1975

TECTONIC SETTING

General Features

Figure 1 is a map of the region of interest. The area just to the west of this map is denoted the "Garm region" by the Soviets; it has the strongest seismicity in the U.S.S.R. (Keilis-Borok, 1960) and recently has been notable for earthquake prediction efforts (Semyenov, 1969). This study will examine crustal seismicity in an area east of Garm in the Northern Pamirs where seismicity is also high. The seismicity in this area is shallow (< 70 km) and runs parallel to the E-W trend of the mountain chain and is probably a result of the ongoing Indian-Eurasian collision (Molnar and Tapponnier, 1975). South of the Pamirs in the Hindu Kush, a vertical zone of intermediate-depth seismic activity suggests that underthrusting of the lithosphere occurred there in the last 10 million years (Molnar et al., 1973). Measurements of vertical and horizontal movements suggest that uplift and thrust faulting are still continuing in the Pamirs.

The Pamirs consist of a high plateau of folded Cenozoic sediments. A large negative Bouguer gravity anomaly of -450 mgal in the Northern Pamirs is associated with relatively large crustal thicknesses (55-65 km) in that region (Kosminskaya et al., 1958).

Keilis-Borok, V. I. (1960), Investigation of the Mechanism of Earthquakes, English translation, American Geophysical Union, Washington, D.C.

Semyenov. A. N. (1969), Variations in the travel time of transverse and longitudinal waves before violent earthquakes, Izvestiya, Phys. Solid Earth, No. 4, 245.

Molnar, P., and P. Tapponnier (1975), Cenozoic tectonics of Asia: effects of a continental collision, Science, 189, 419.

Molnar, P., T. Fitch, and F. Wu (1973), Fault plane solutions of shallow earthquakes and contemporary tectonics in Asia, Earth and Planetary Science Letters, 19, 101.

Kosminskaya, I., G. Mikhota, and Y. Tulina (1958), Crustal structure of the Pamir-Alai zone from seismic depth-sounding data, Izvestiya, Geophysics Series, 673.

Source Mechanisms of Earthquakes

NEIS epicenters for events in this area from January 1971 through February 1975 are shown in Figure 1. The geologic faults in this figure were inferred from a satellite photomosaic of the area and published geologic or tectonic maps. Most of the earthquakes are associated with the Pamir thrust fault and the other thrust faults which lie parallel to it (Shirokova, 1967). In the northern part of this region, some of the events lie close to a left-lateral strike-slip fault. The compressive stress component for events along the Pamir thrust fault is generally directed perpendicular to the structural trend of the Pamir Mountain system (Ritsema, 1966). Molnar et al. (1973) found both thrust faulting and strike-slip faulting associated with the Pamir thrust. In general, however, the pattern of fault plan solutions is very complex and unpredictable and has little correlation with known faults (Keilis-Borok, 1960).

Velocity Model

Seismic studies in the Pamirs report an average crustal thickness of $>$ 50 km (Kosminskaya et al., 1958) with depths to 65 km indicated. Table 1 shows a general crustal and upper mantle velocity structure derived from deep seismic sounding in the area of interest; the actual structure varies rapidly over the area encompassing the earthquakes we have selected for this study though. Seismological data show that a slight low-velocity zone with Vp ~

Shirokova, E. (1967), General features in the orientation of principal stresses in earthquake foci in the Mediterranean-Asian seismic belt, Izvestiya, Physics of the Solid Earth, 12, 12.

Ritsema, A. (1966), The fault-plane solutions of earthquakes of the Hindu-Kush center, Tectonophysics, 3, 147.

Molnar, P., T. Fitch, and F. Wu (1973), Fault plane solutions of shallow earthquakes and contemporary tectonics in Asia, Earth and Planetary Science Letters, 19, 101.

Keilis-Borok, V. I. (1960), Investigation of the Mechanism of Earthquakes, English translation, American Geophysical Union, Washington, D.C.

Kosminskaya, I., G. Mikhota, and Y. Tulina (1958), Crustal structure of the Pamir-Alia zone from seismic depth-sounding data, Izvestiya Geophysics Series, 673.

TABLE I

Velocity Structure in the Pamirs

Thickness (km)	P Velocity (km/sec)	Density (gm/cm^3)
2	5.0	2.6
30	5.5	2.7
30	6.5	3.1
mantle	8.1	3.3

7.9 km/sec extended from 10 to 20 km below the Moho to about 180 km depth (Aliev et al., 1976, and Vinnik and Lukk, 1974). This contrasts with the much more pronounced low-velocity zone under the western United States where Vp ~ 7.7 km/sec (Archambeau et al., 1969). There is evidence from pP reflections (Vinnik and Godzikovskaya, 1973) of a zone of higher than normal upper-mantle attenuation to the south and east of the area encompassing the earthquakes of this report, but this same data indicated that attenuation is less than normal under the Pamirs itself.

Aliev, S., N. Beliaevsky, E. Butovskaya, B. Volvovsky, I. Volvovsky, G. Krasnopevtseva, V. Pak, M. Polshkov, V. Rubailo, V. Sallogub, B. Tal-Virsky, F. Tregub, I. Khamrabayev, and G. Kharechko (1976), The seismic experiment in the Northern Pamirs, in Geodynamics: Progress and Prospects, ed. C. Drake, American Geophysical Union.

Vinnik, L. P., and A. A. Lukk (1974), Lateral inhomogeneities of the upper mantle under the Pamir and Hindu Kush, Izv., Earth Physics, No. 1, 9.

Archambeau, C., E. Flinn, and D. Lambert (1969), Fine structure of the upper mantle, J. Geophys, Res., 74, 5825.

Vinnik, L. P., and A. A. Godzikovskaya (1973), Lateral variations of the absorption by the upper mantle beneath Asia, Izv., Earth Physics, No. 1, 3.

DATA

Earthquake Selection

For this study earthquakes were selected which had low reported M_s for their m_b so that these events fall close to the explosion population on an M_s-m_b graph. The NEIS list suggests both shallow and intermediate depth events in this region. Most of the intermediate depth activity takes place south of the area of interest in the Hindu Kush. Shallow depth events (less than 70 km) predominate in the Northern Pamirs. Most of the seismic activity in the Northern Pamirs is associated with the Pamir thrust fault, as shown in Figure 1. The earthquakes chosen were limited to the years 1971 to 1975 so that we could utilize the data from the large seismic arrays and the HGLP network. We selected a total of 11 earthquakes as listed in Table II and shown in Figure 1. Table II also lists the depths determined from pP observations at LASA and NORSAR. All of the events are located within the crust. Events 5 through 11 are all closely located, and although no pP data was available at LASA or NORSAR for event 10, a pP observation at SHI implies a focal depth of 25 km.

Explosion Selection

The Pamir earthquakes were compared to the Kazakh explosions which lie to the northwest and northeast of the Pamirs. We selected a total of 10 explosions as listed in Table III.

Seismic Stations

Digital data from the three arrays ALPA, LASA, and NORSAR and from the available HGLP stations and film data from selected WWSSN stations were gathered for these events. The LASA AO subarray and NORSAR C3 subarray short-period P recordings are shown in Figure 2. WWSSN stations were selected on the basis of magnification and proximity to the region of study, and it is unlikely that the stations not used here would significantly add to the data base for these Pamir events.

Table II

NEIS Parameters for Pamir Earthquakes

Event	Date	Origin Time	EPICENTER Latitude N	EPICENTER Longitude E	m_b	DEPTH NEIS	DEPTH NORSAR	DEPTH LASA
1	24 Nov 71	08 23 24.6	38.692	73.350	5.1	33	10	
2	12 Dec 71	22 27 41.1	39.482	73.228	4.8	33	17	
3	03 Jan 73	15 05 16.6	39.119	72.097	4.8	33	19	19
4	20 Feb 74	11 43 03.9	40.661	73.223	5.1	25	20	20
5	11 Aug 74	08 02 54.0	39.288	73.922	5.1	12	14	8
6	11 Aug 74	09 08 58.5	39.236	73.859	5.1	29	12	12
7	11 Aug 74	23 18 58.3	39.462	73.604	5.1	33	15	12
8	14 Aug 74	22 06 52.9	39.195	73.865	5.0	33	30	
9	21 Aug 74	18 08 29.0	39.266	73.933	4.9	33	7	6
10	23 Aug 74	16 26 30.5	39.272	73.736	4.9	33		
11	07 Sep 74	15 46 30.9	39.286	73.896	4.9	33		16

Table III

NEIS Parameters for Kazakh Explosions

Event	Date	Origin Time	EPICENTER Latitude N	EPICENTER Longitude E	m_b
1	22 Mar 71	04 32 57.8	49.744	78.185	5.8
2	29 Nov 71	06 02 57.1	49.758	78.126	5.5
3	30 Dec 71	06 20 57.7	49.750	78.130	5.8
4	10 Feb 72	05 02 57.3	49.986	78.886	5.5
5	24 Nov 72	09 59 57.8	51.843	64.152	5.2
6	15 Aug 73	01 59 57.8	42.711	67.410	5.3
7	19 Sep 73	02 59 57.2	45.635	67.850	5.2
8	30 Sep 73	04 59 57.5	51.608	54.582	5.2
9	25 Jun 74	03 56 57.6	49.889	78.115	4.7
10	07 Dec 74	05 59 56.9	49.908	77.648	4.7

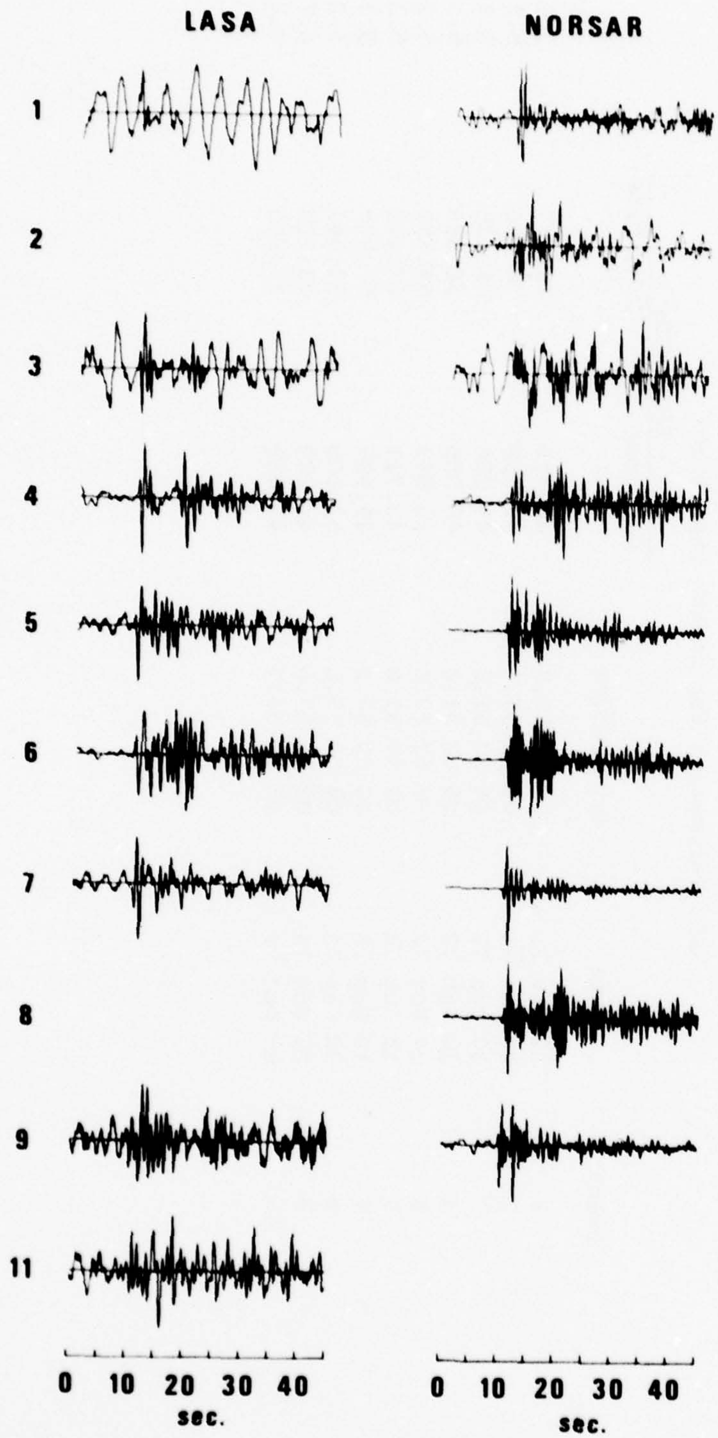

Figure 2. LASA and NORSAR short-period P recordings for the Pamir events studied

SIGNAL ANALYSIS

Source Effects

We wanted initially to identify a source mechanism for each event so that we could predict the radiation pattern for body-wave and surface-wave phases. Determination of the fault planes for earthquakes whose magnitudes are below 6.0 is generally not reliable with teleseismic data, and all our earthquakes have m_b less than 6. Few clear first motions were recorded from the data we had collected. ISC bulletin data was available for events 1 through 4; only events 3 and 4 had sufficient numbers of first motions to attempt a focal mechanism plot. We have plotted the ISC (International Seismological Center) first motions for events 3 and 4 in Figure 3. Unfortunately, the short-period data were not consistent and it is impossible on the basis of the plots alone to determine fault planes because dilatational and compressional first motions do not separate.

Corner frequencies and seismic moments for our Pamir events have been estimated from short-period LASA and NORSAR spectra. The spectra are shown in Figure 4. These spectra are from the phased beams of the A0 short-period subarray at LASA and C3 short-period subarray at NORSAR. The sample length was 6.4 seconds. The signals have been tapered, and the instrument response was removed from the signal and noise spectra; but noise spectra have not been subtracted from the signal spectra. Attenuation was removed from the spectra by multiplying by the factor $\exp[\pi f t^*]$ with a t^* of .53 for a ω^{-2} source model and .34 for ω^{-3} source models at LASA and t^* of .00 for ω^{-2} and ω^{-3} source models at NORSAR. The basis for these t^* values will be shown later in this report. Corner frequencies were estimated with the assumption of complete stress drop over a circular or square fault plane and a ω^{-2} or ω^{-3} asymptotic relation at high frequencies. Note that, for many of the spectra of Figure 4, dashed lines are used to indicate the long-period level and the corner frequency. This indicates our lack of confidence in the estimates. Occasionally we computed spectra for 25.6-second windows for those cases where the signal-to-noise ratio was high. For these cases the shape of the spectra were sufficiently identical to those for the 6.4-second windows that we have not shown them.

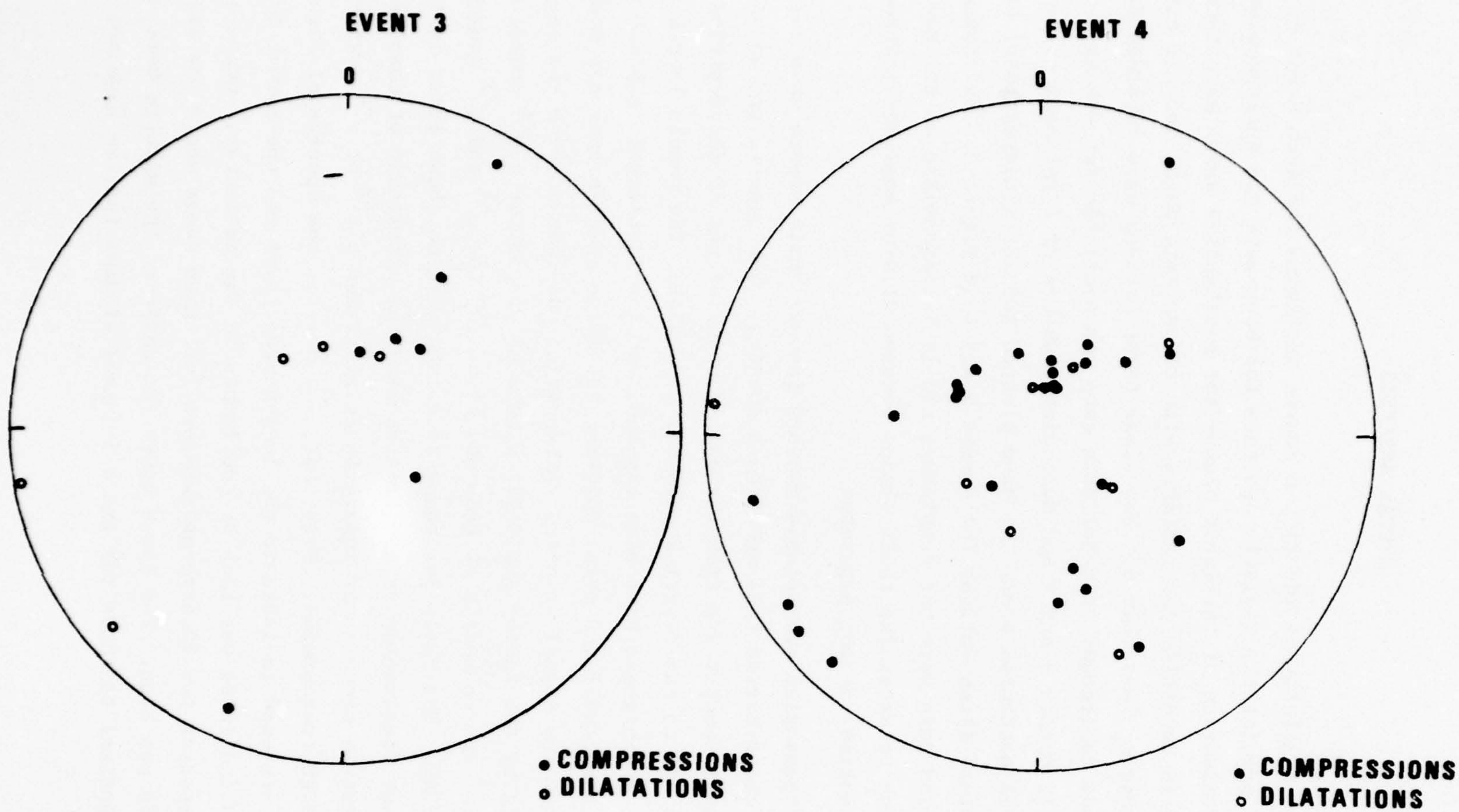

Figure 3. First motions for Pamir earthquakes in the lower half of the focal sphere (Wulff net)

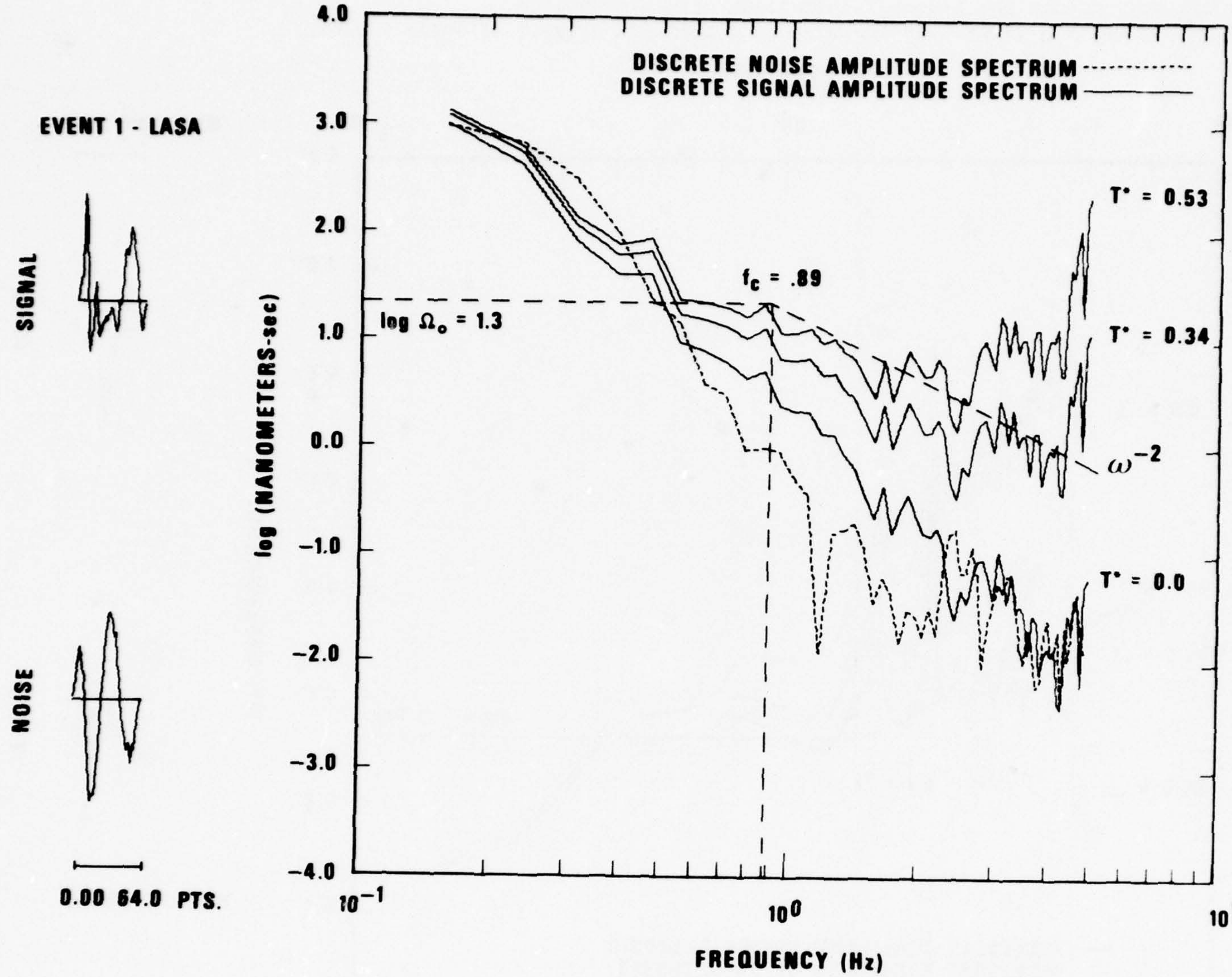

Figure 4. LASA AO and NORSAR C3 subarray spectra of P waves from Pamir earthquakes with instrument response and attenuation removed.

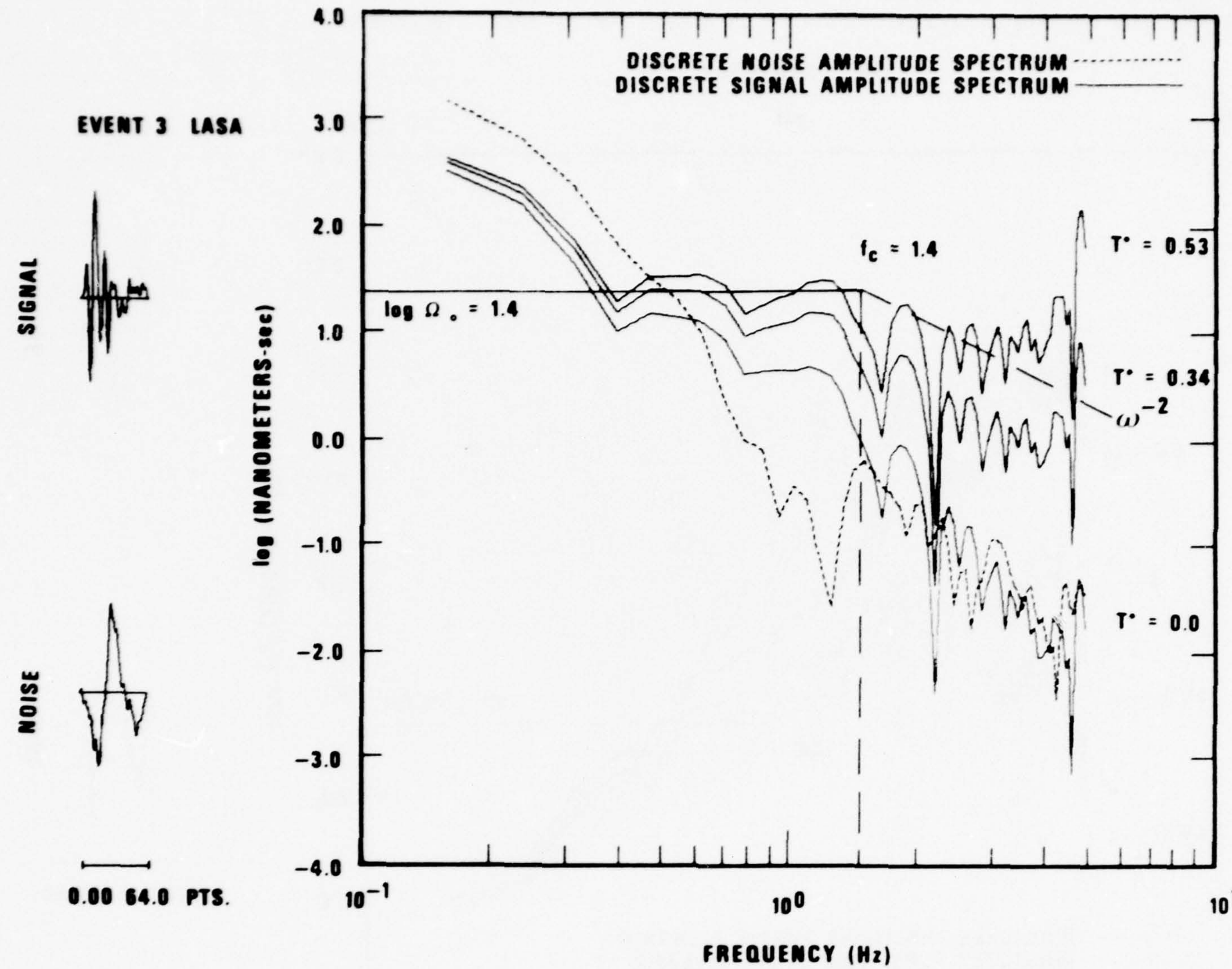

Figure 4 (cont.) LASA AO and NORSAR C3 subarray spectra of P waves from Pamir earthquakes with instrument response and attenuation removed.

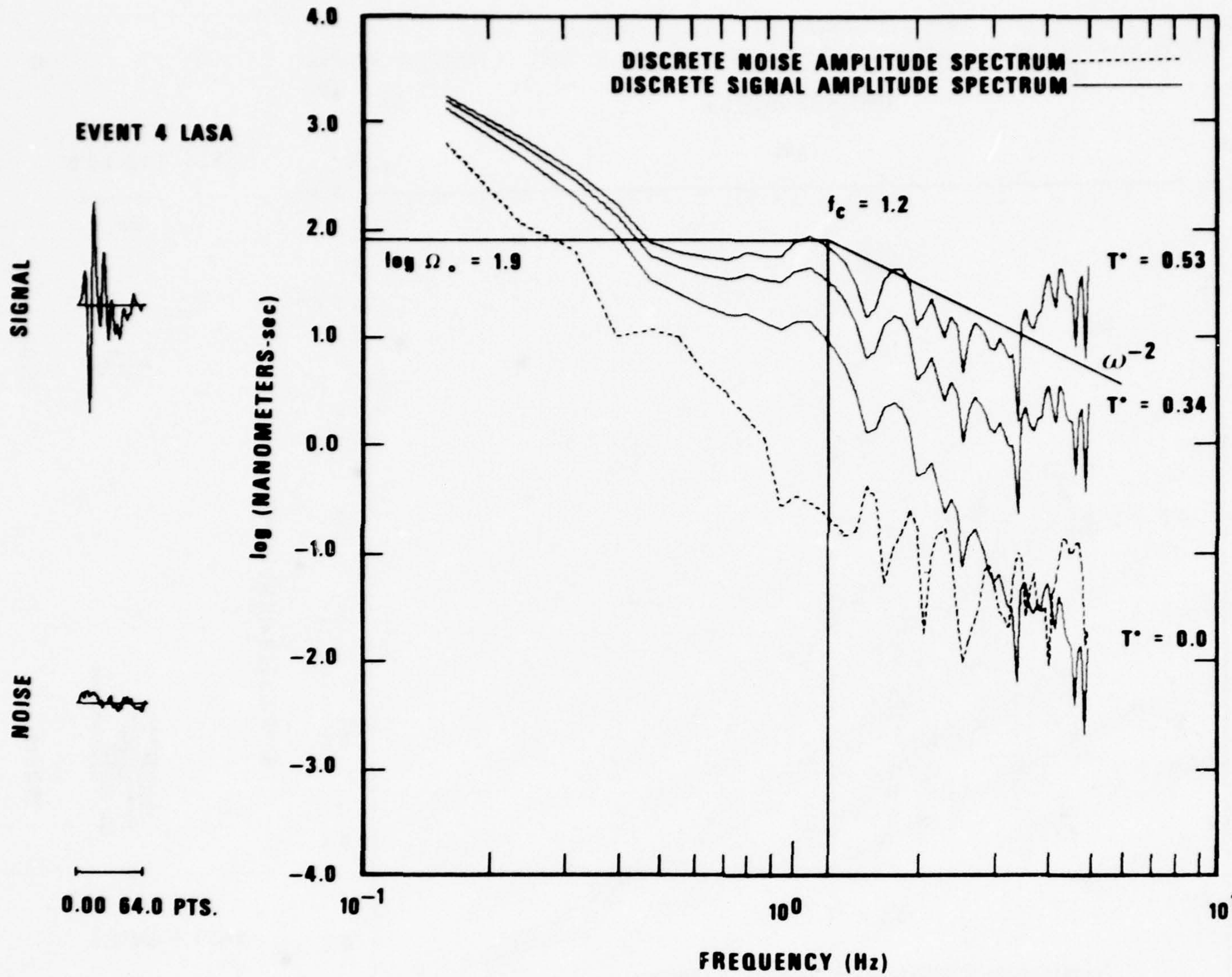

Figure 4 (cont.) LASA AO and NORSAR C3 subarray spectra of P waves from Pamir earthquakes with instrument response and attenuation removed.

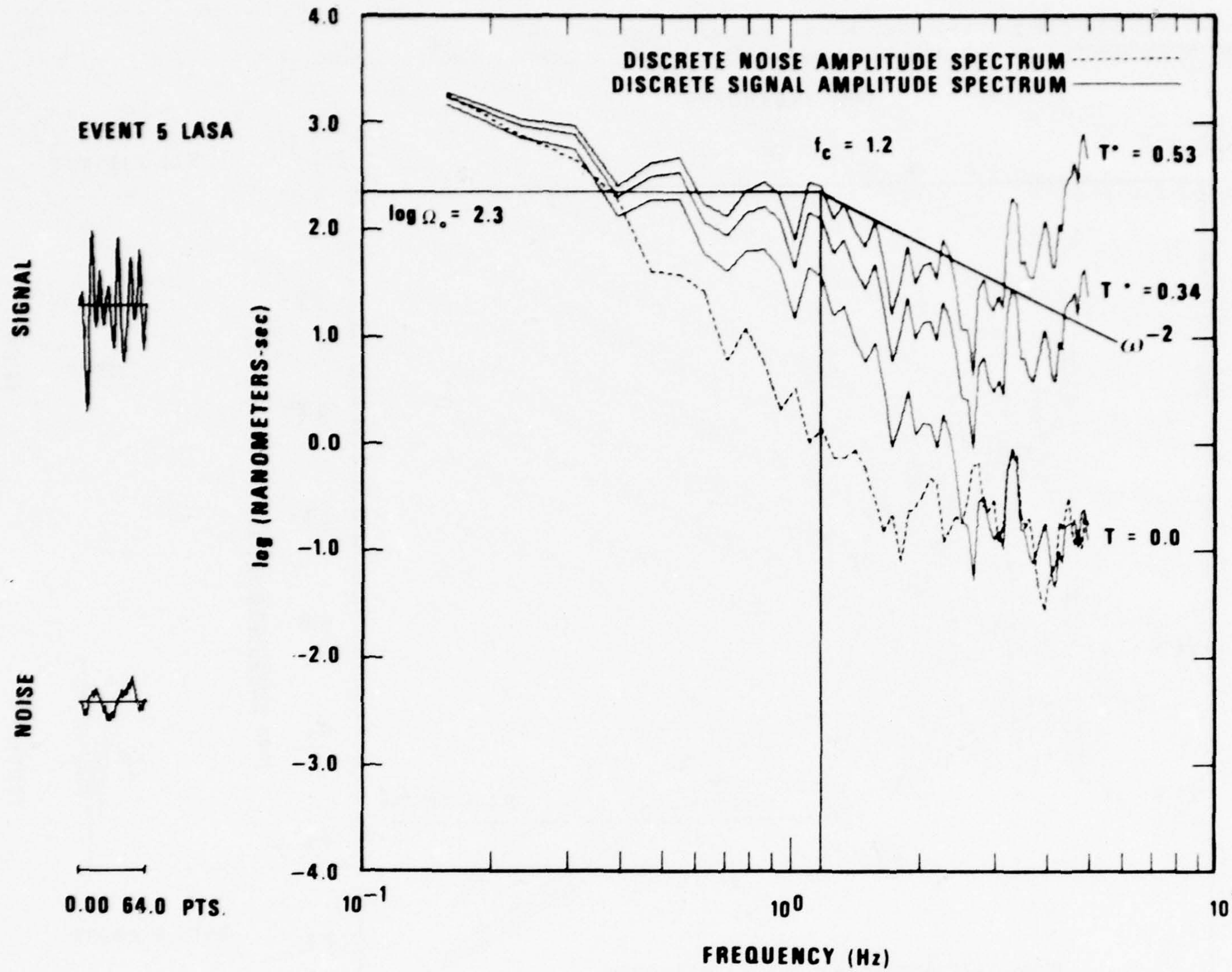

Figure 4 (cont.) LASA AO and NORSAR C3 subarray spectra of P waves from Pamir earthquakes with instrument response and attenuation removed.

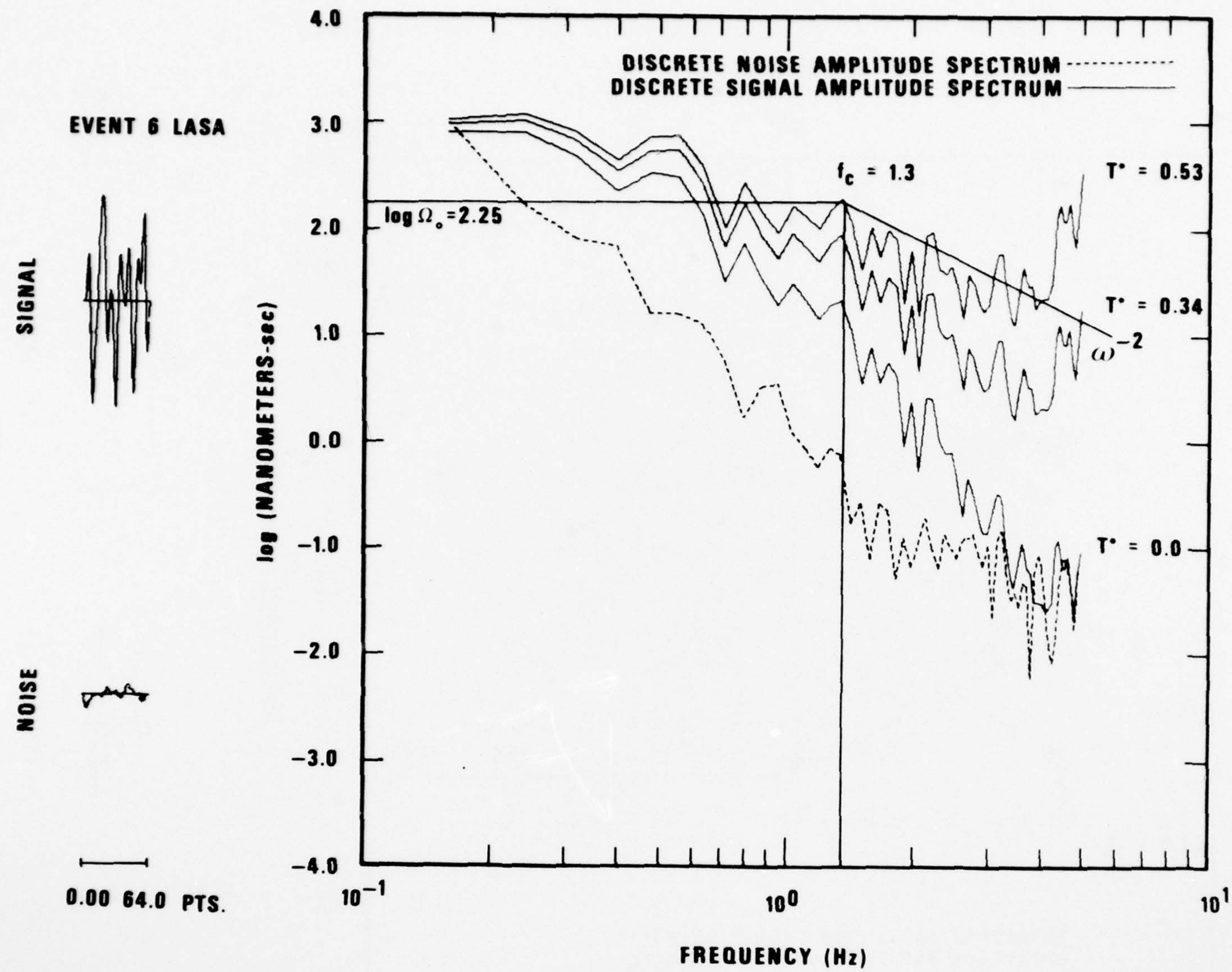

Figure 4 (cont.) LASA AO and NORSAR C3 subarray spectra of P waves from Pamir earthquakes with instrument response and attenuation removed.

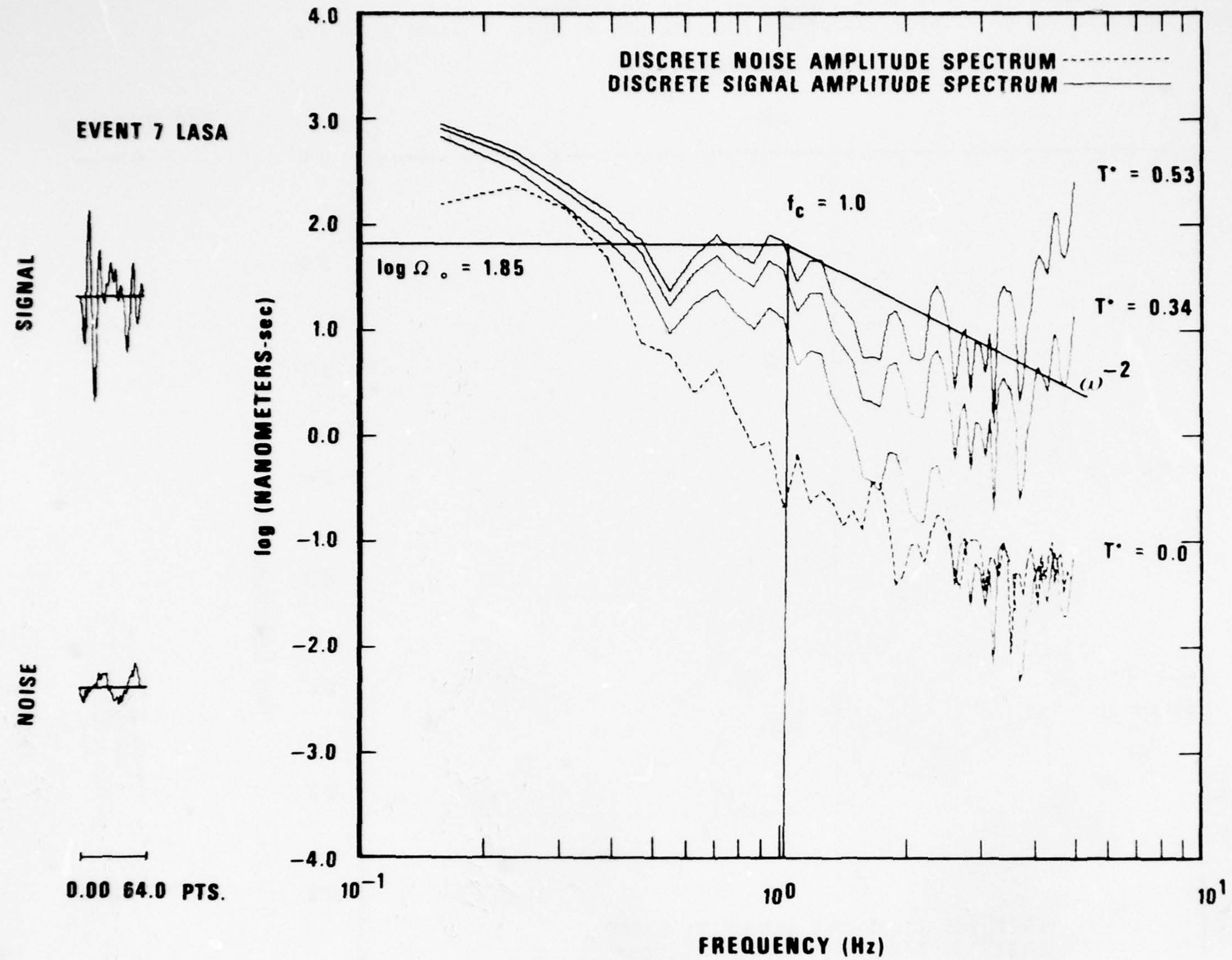

Figure 4 (cont.) LASA AO and NORSAR C3 subarray spectra of P waves from Pamir earthquakes with instrument response and attenuation removed.

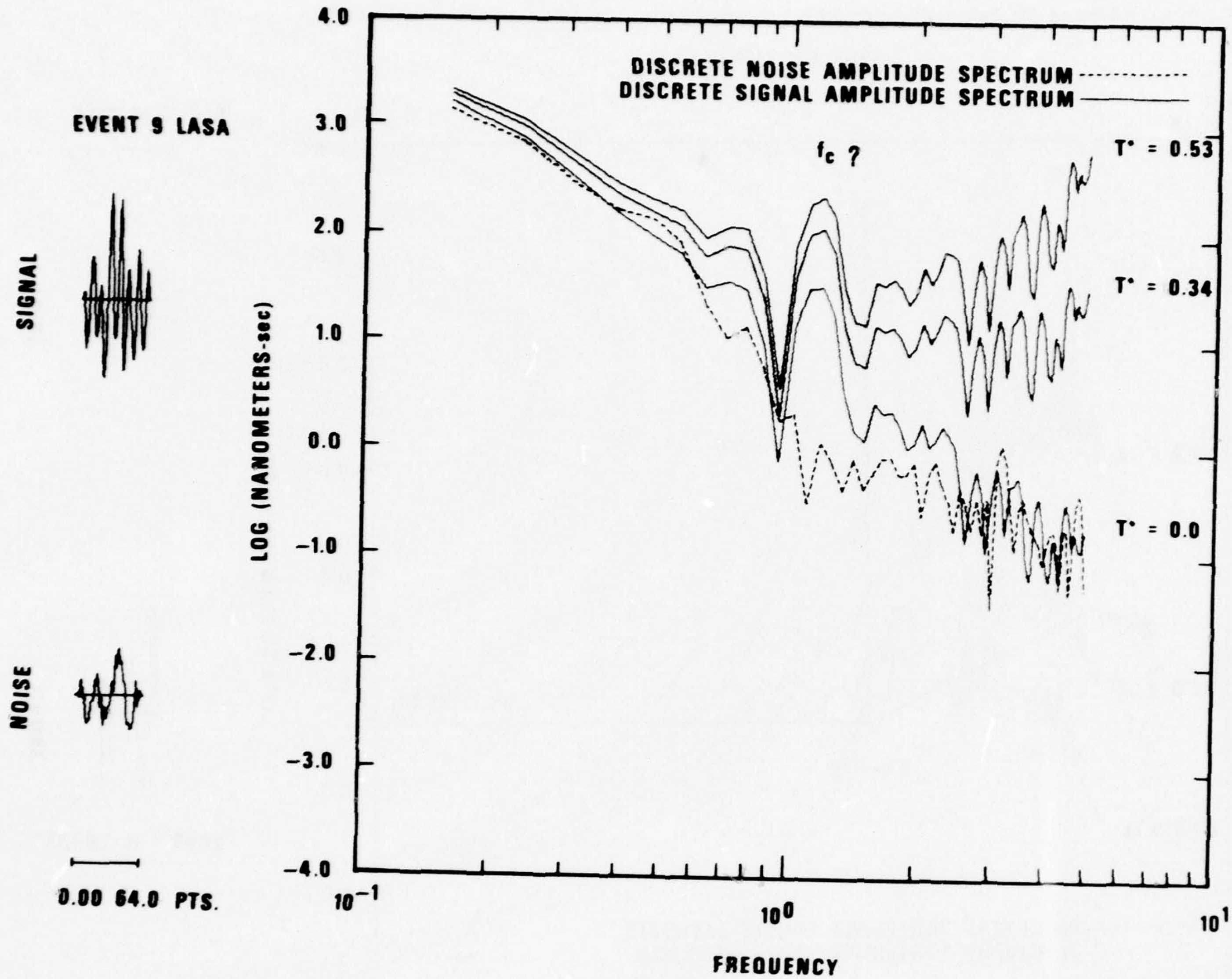

Figure 4 (cont.) LASA AO and NORSAR C3 subarray spectra of P waves from Pamir earthquakes with instrument response and attenuation removed.

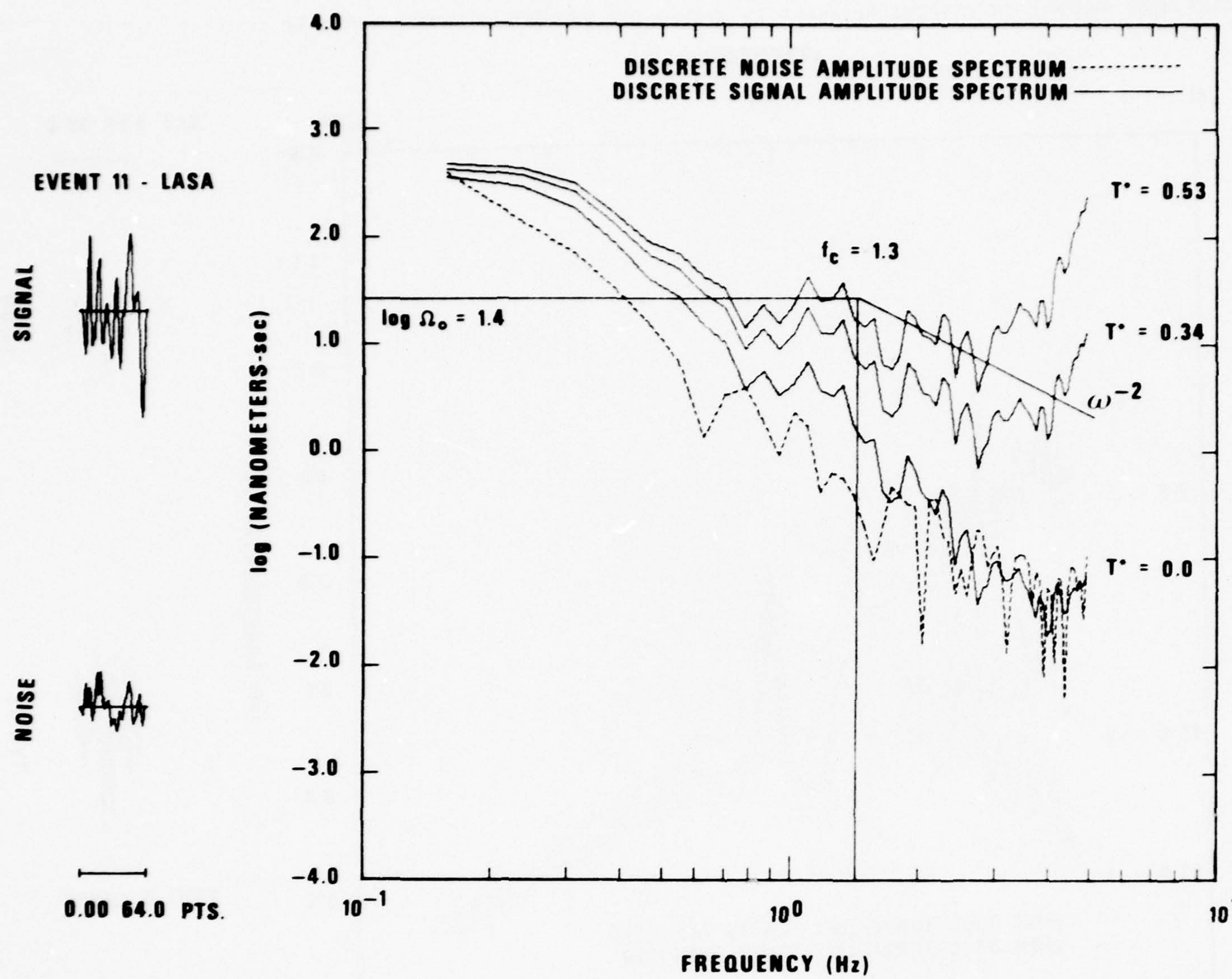

Figure 4 (cont.) LASA AO and NORSAR C3 subarray spectra of P waves from Pamir earthquakes with instrument response and attenuation removed.

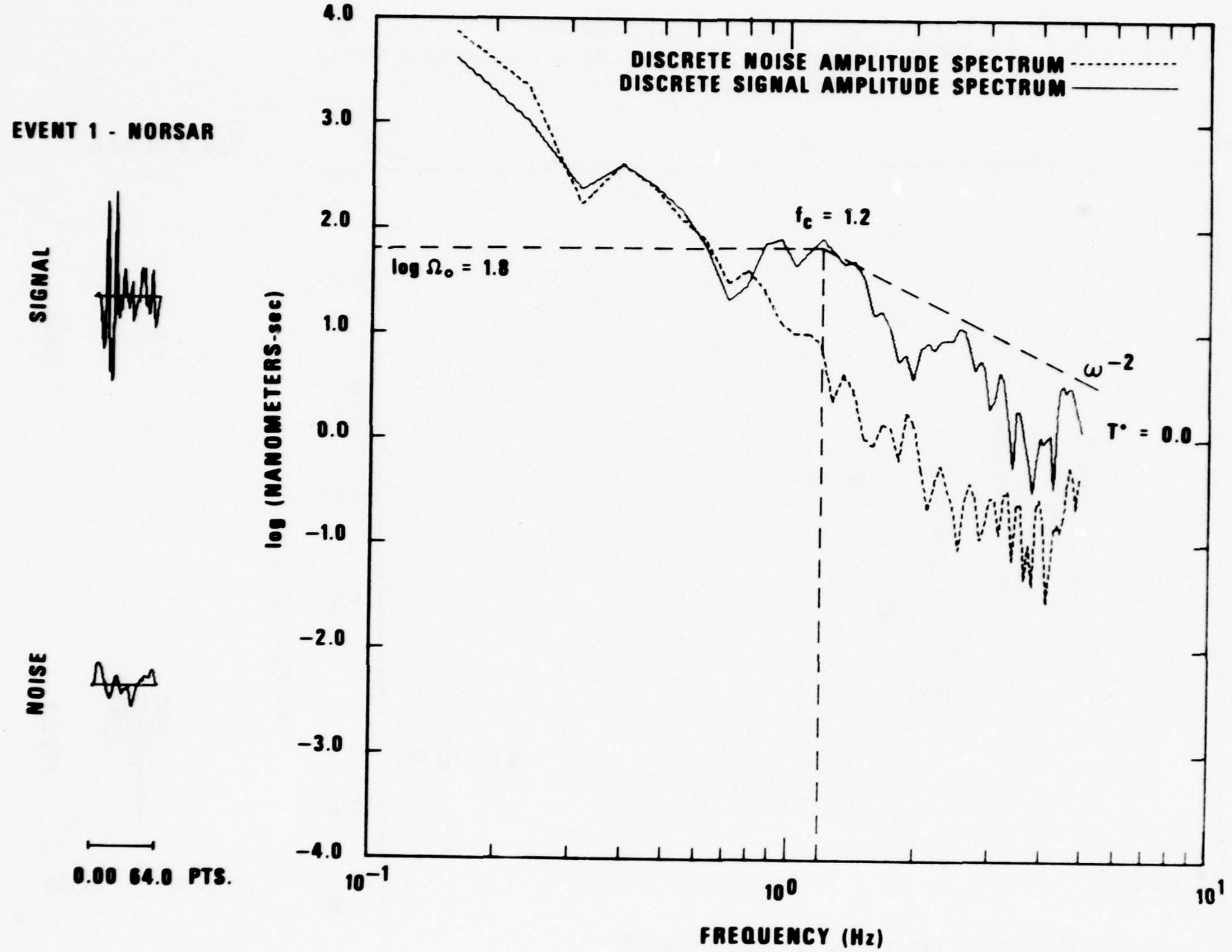

Figure 4 (cont.) LASA AO and NORSAR C3 subarray spectra of P waves from Pamir earthquakes with instrument response and attenuation removed.

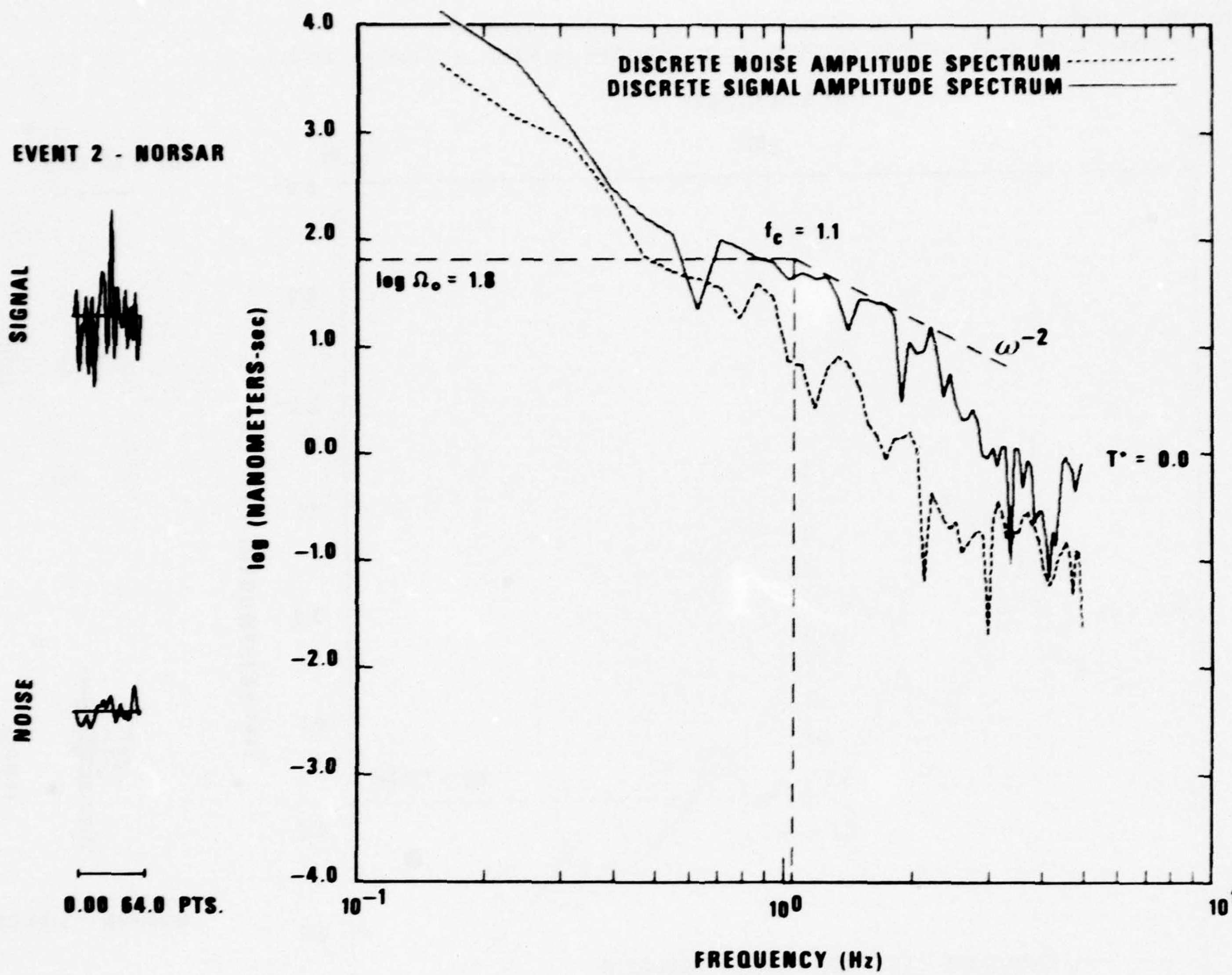

Figure 4 (cont.) LASA AO and NORSAR C3 subarray spectra of P waves from Pamir earthquakes with instrument response and attenuation removed.

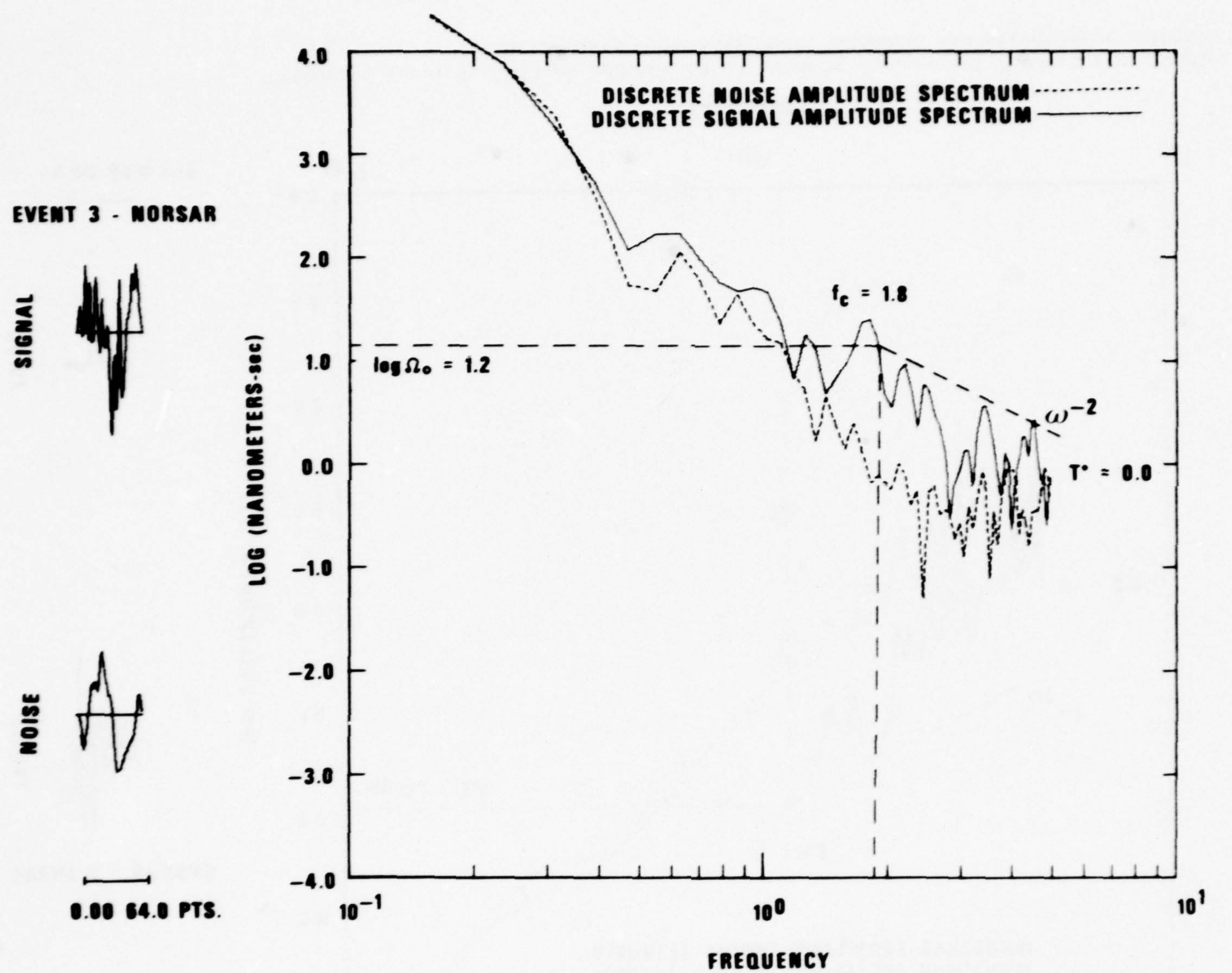

Figure 4 (cont.) LASA AO and NORSAR C3 subarray spectra of P waves from Pamir earthquakes with instrument response and attenuation removed.

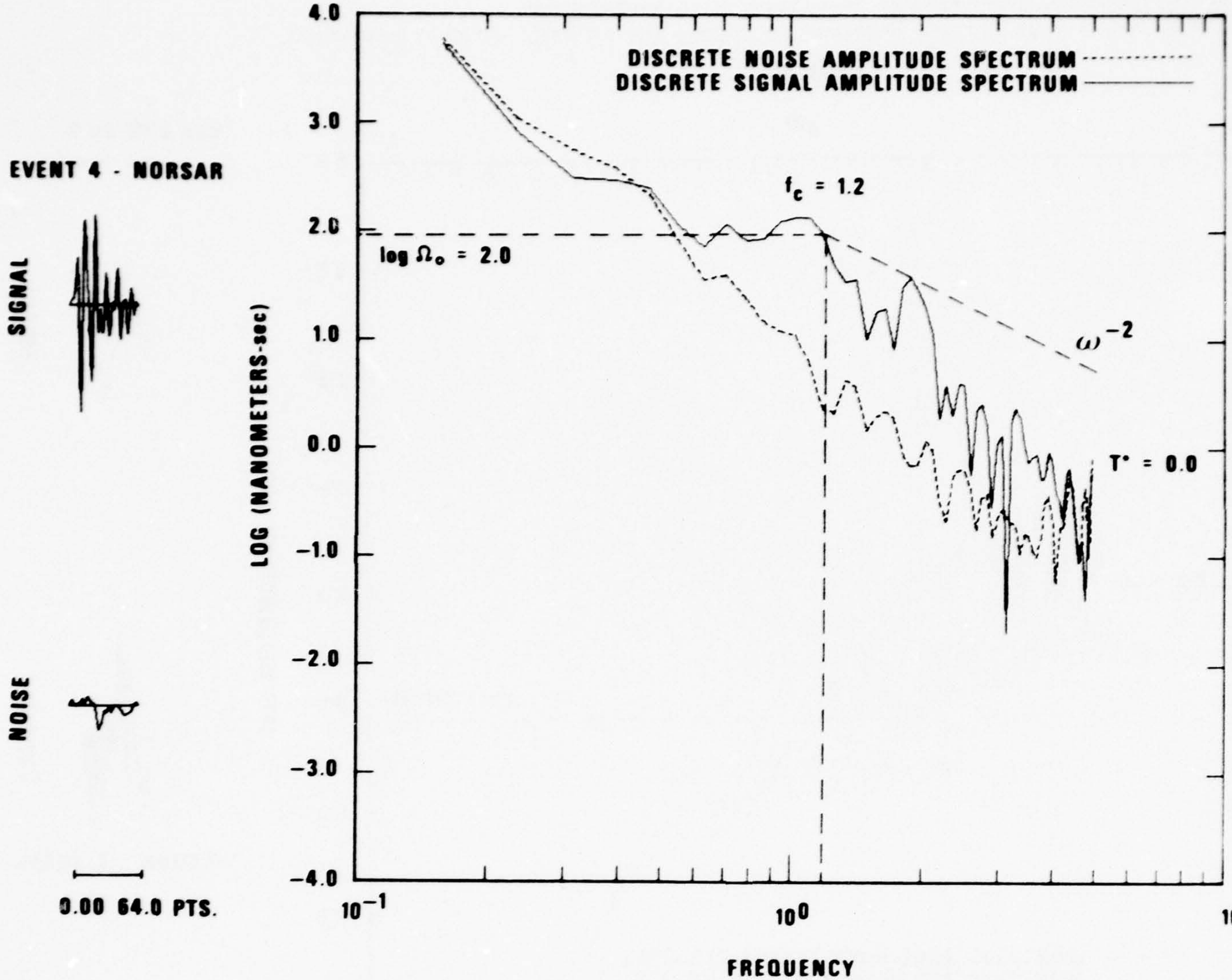

Figure 4 (cont.) LASA A0 and NORSAR C3 subarray spectra of P waves from Pamir earthquakes with instrument response and attenuation removed.

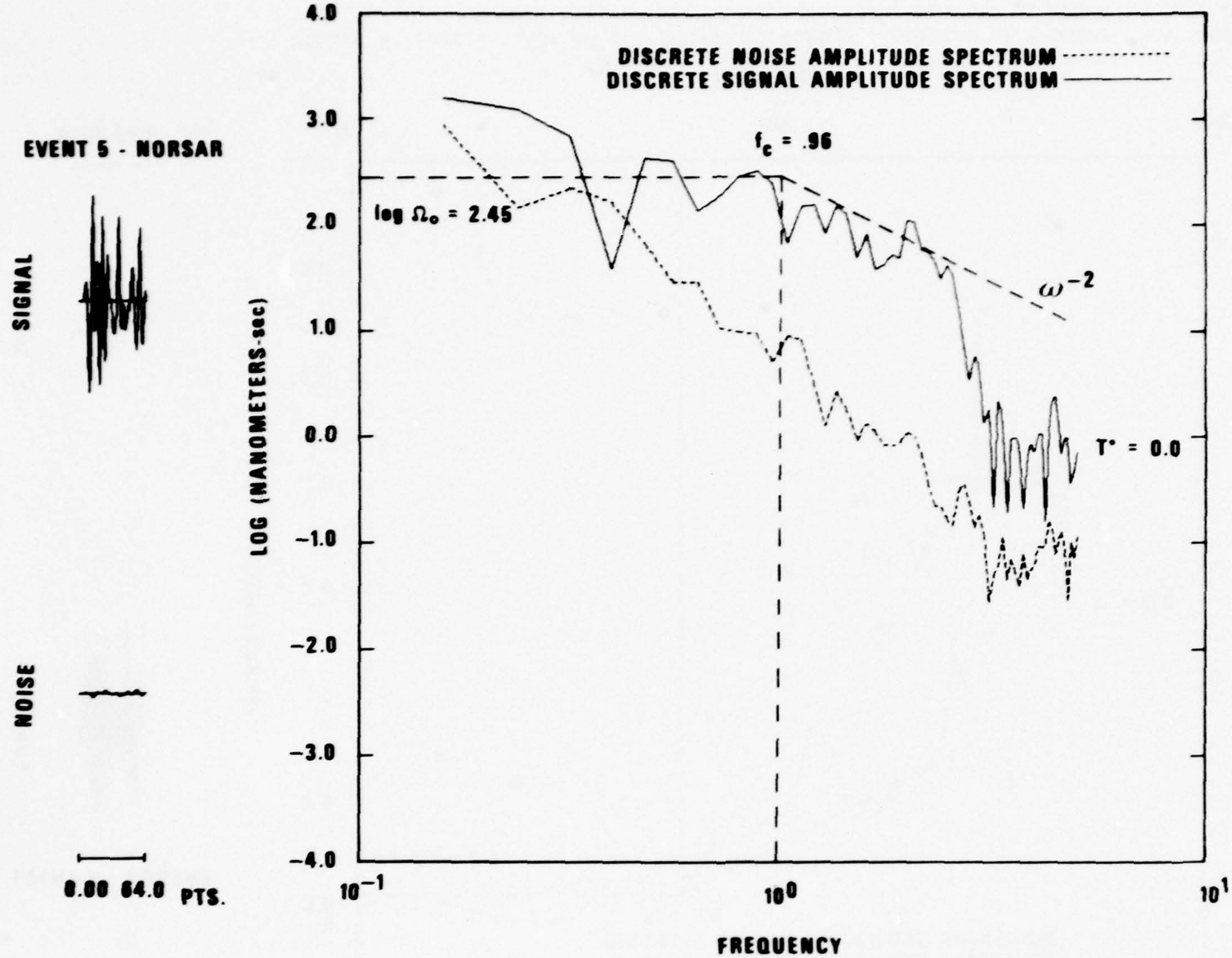

Figure 4 (cont.) LASA AO and NORSAR C3 subarray spectra of P waves from Pamir earthquakes with instrument response and attenuation removed.

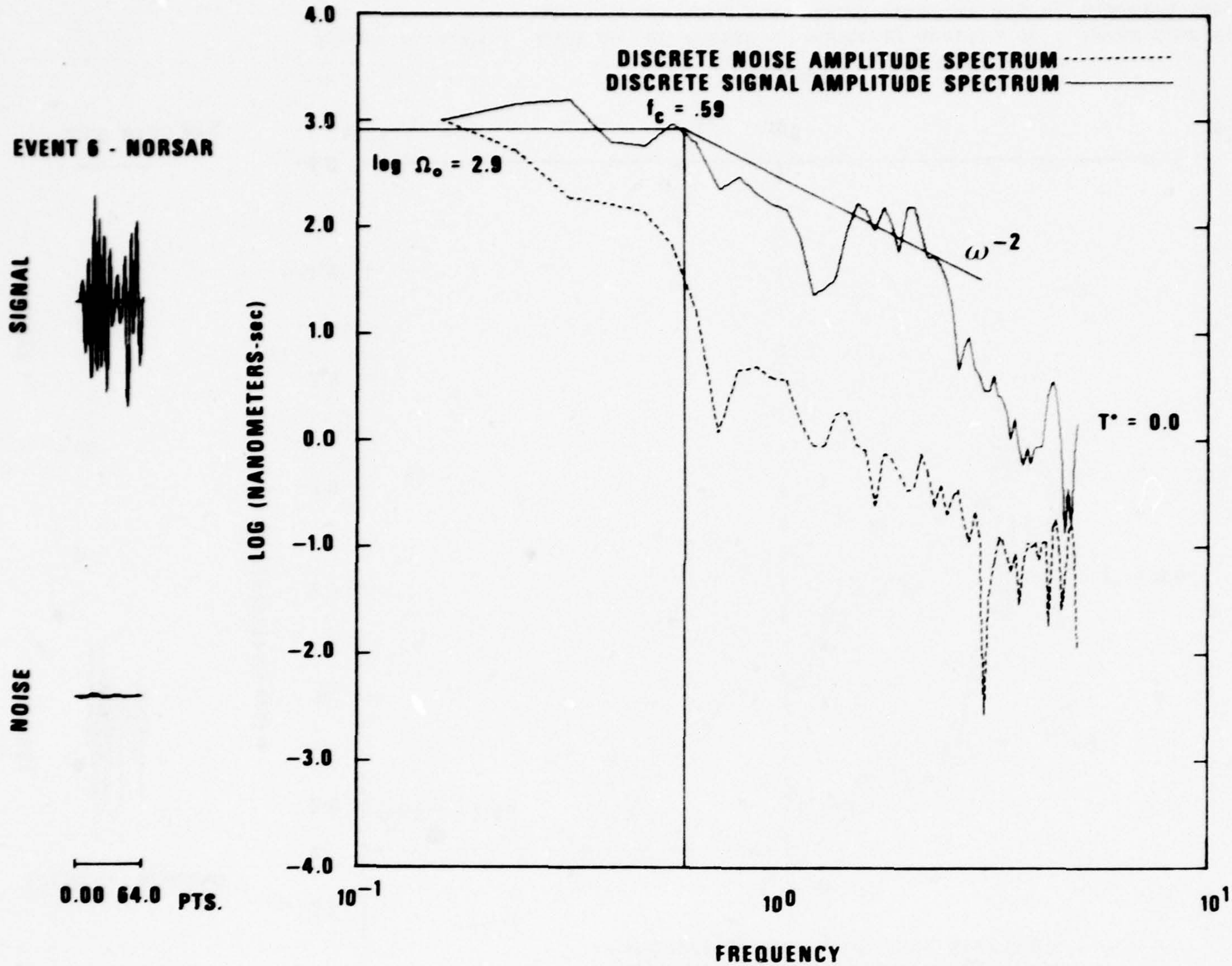

Figure 4 (cont.) LASA AO and NORSAR C3 subarray spectra of P waves from Pamir earthquakes with instrument response and attenuation removed.

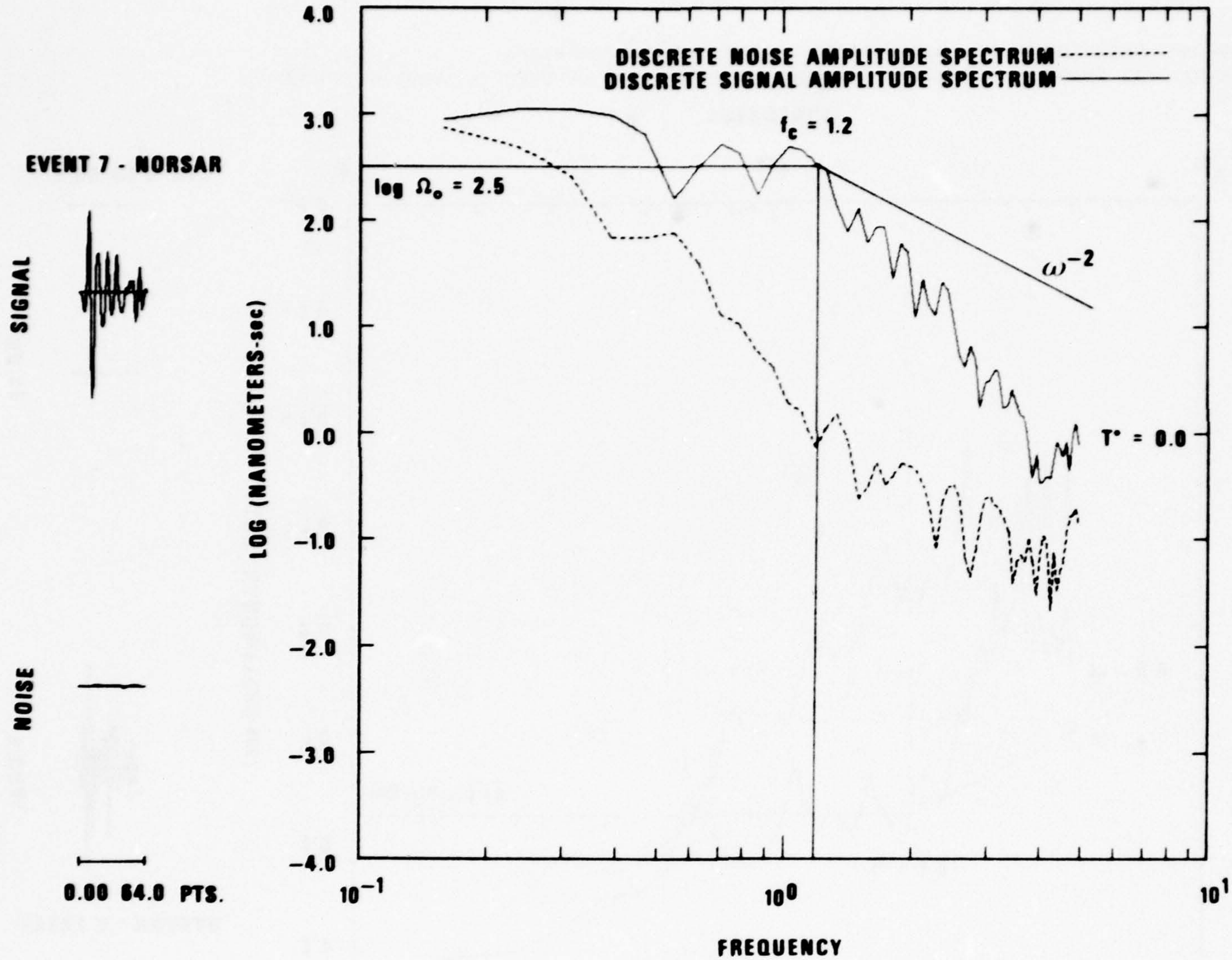

Figure 4 (cont.) LASA AO and NORSAR C3 subarray spectra of P waves from Pamir earthquakes with instrument response and attenuation removed.

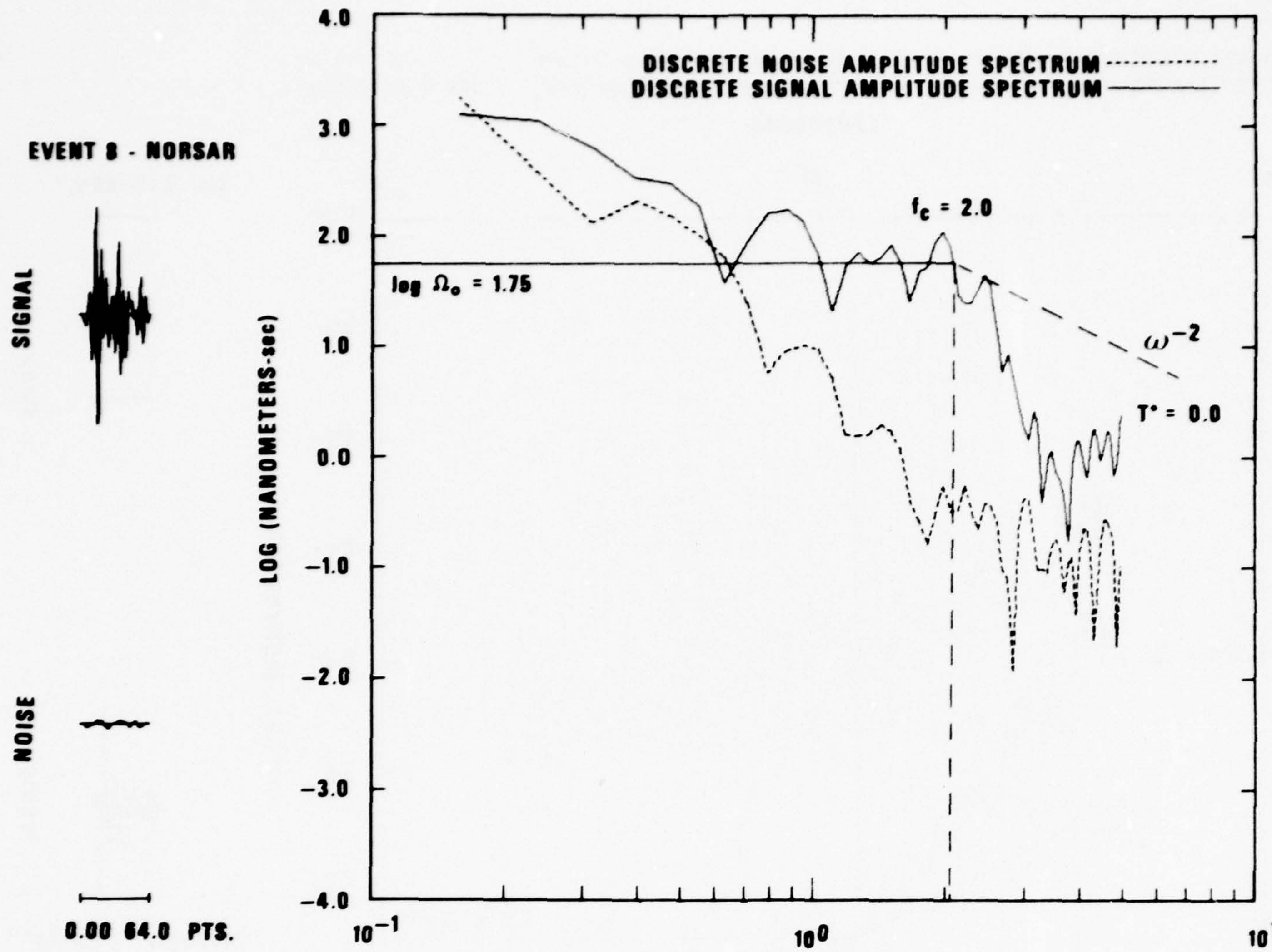

Figure 4 (cont.) LASA AO and NORSAR C3 subarray spectra of P waves from Pamir earthquakes with instrument response and attenuation removed.

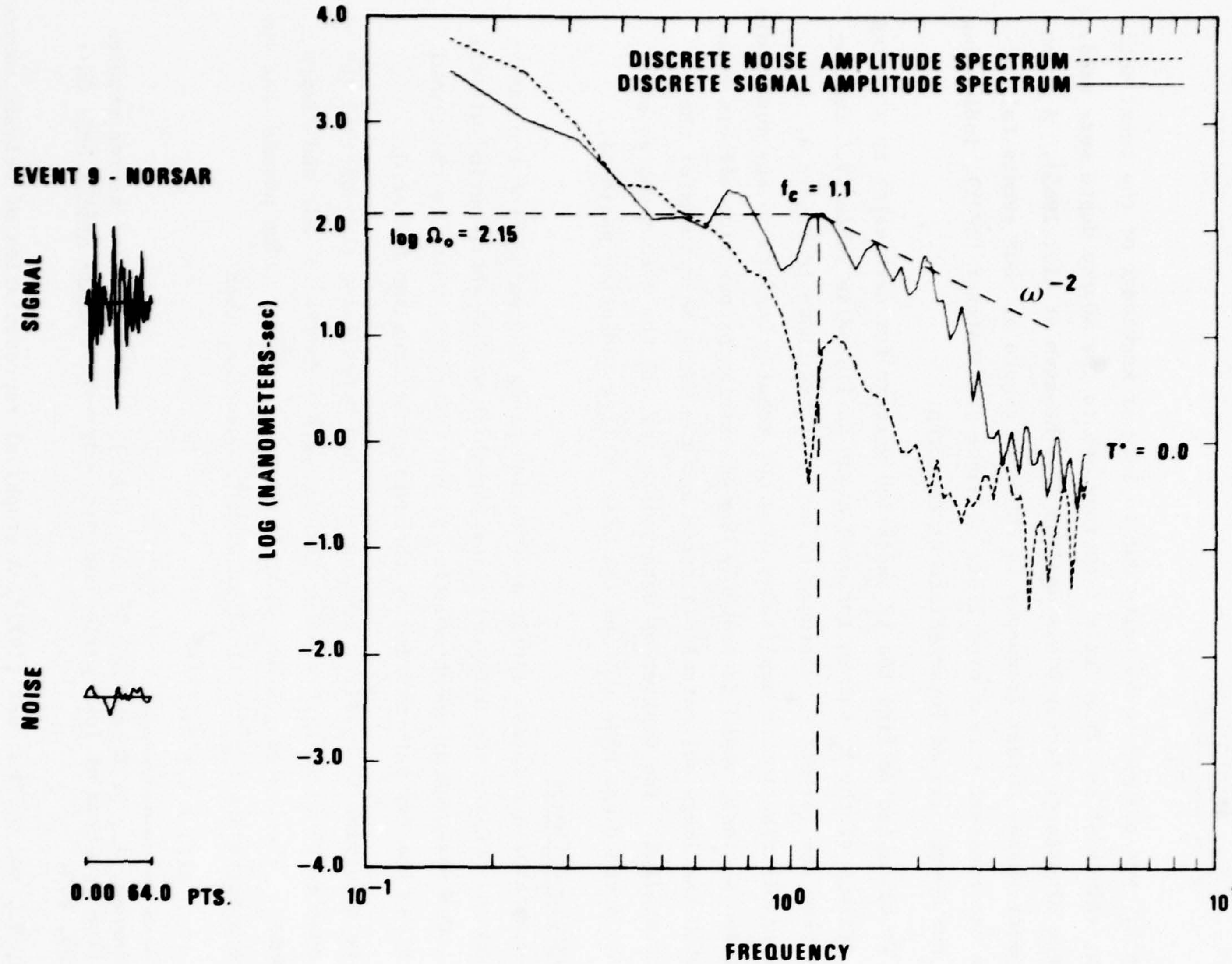

Figure 4 (cont.) LASA AO and NORSAR C3 subarray spectra of P waves from Pamir earthquakes with instrument response and attenuation removed.

Seismic moment was calculated from the long-period body-wave spectral displacement levels $|\Omega_o|$ estimated in Figure 4 using the relation

$$M_o = \frac{4\pi\rho\alpha^3 D|\Omega_o|}{R_{\theta\phi}}$$

where $R_{\theta\phi}$ was assumed to be unity due to lack of knowledge of the focal mechanism, values of $\rho\alpha^3$ from Table I appropriate to the source depth were used, and the divergence factor D was applied (Ben-Menahem et al., 1965). A graph of moment versus corner frequency is shown in Figure 5. Our events fall between the constant stress drop lines of Hanks and Thatcher (1972), indicating that our events are of intermediate stress drop.

We attempted to find the LR radiation pattern for each event by plotting the antilogs of the M_s values for each event as listed in Table IV. The results from the largest M_s earthquake, event 6, are shown in Figure 6. The observed distribution of amplitudes does not readily conform to any quadripole radiation pattern, which is probably due to varying propagation effects coupled with the large epicentral distances and the small magnitudes of the events studied. The scatter of data points for all the events was so poor that no attempt was made to find the best-fitting radiation patterns.

Propagation Effects

We measured relative mantle attenuation along the paths from the Pamirs to LASA and NORSAR, the only two sites for which we had short-period digital data. Our measurement of attenuation is the factor t*, which is the travel time along the ray path divided by the average attenuation factor Q.

We determine t* by first summing and then normalizing the observed (t* = 0.0) spectra shown in Figure 4 for the two paths--Pamirs to LASA and Pamirs to NORSAR. These averages are shown in Figure 7 and 8. If we assume that the source spectra has a f^{-2} falloff at high frequencies, then

$$A(f) \simeq S \cdot f^{-2} \cdot e^{-\pi f t^*}$$

Ben-Menahem, A., S. Smith, and T. Teng (1965), A procedure for source studies from spectrum of long-period seismic body-waves, Bull. Seism. Soc. Am., 55, 203.

Hanks, T., and W. Thatcher (1972), A graphical representation of seismic source parameters, J. Geophys. Res., 77, 4393.

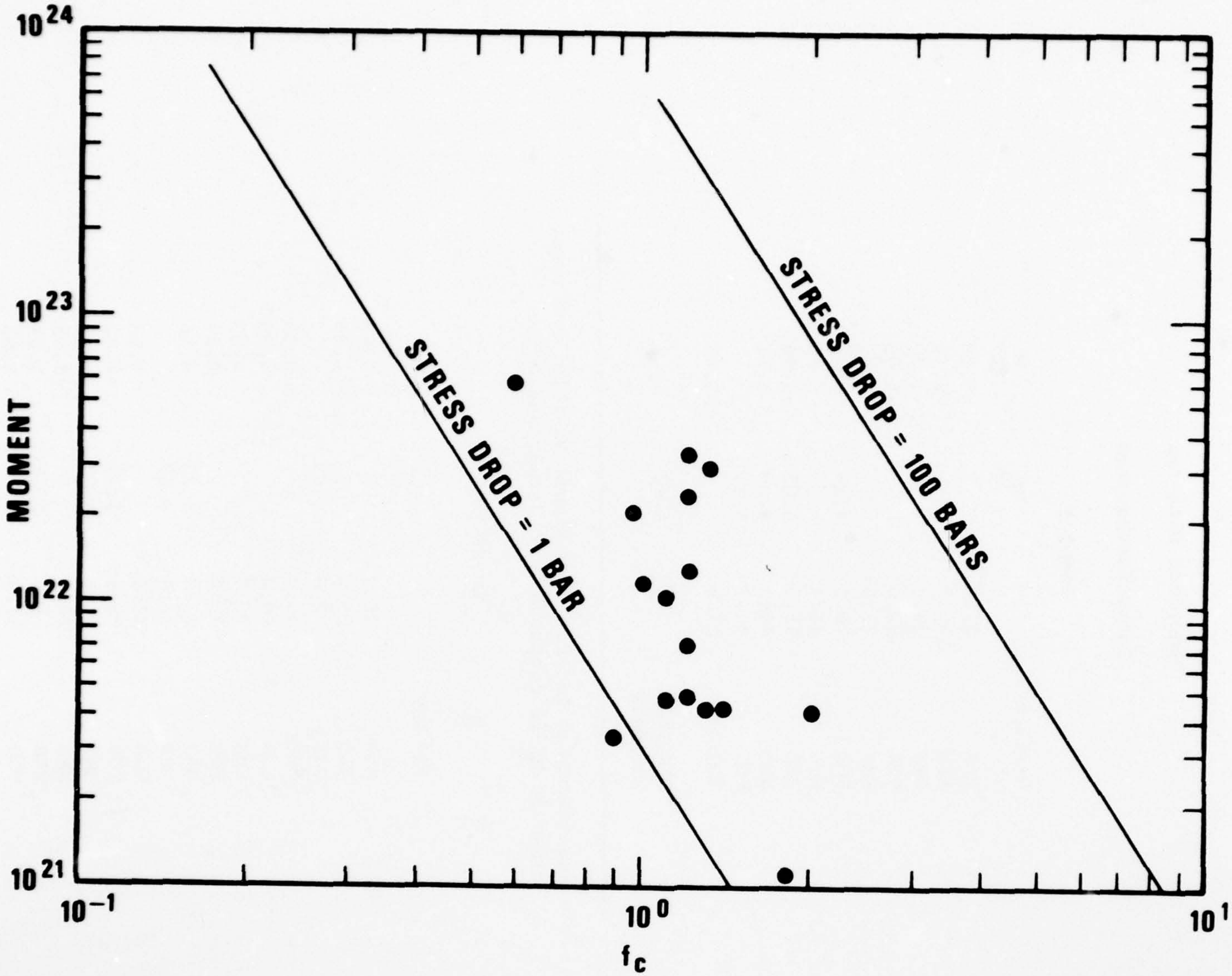

Figure 5. Seismic moment versus corner frequency for Pamir earthquakes from LASA and NORSAR P recordings

Table IV

Magnitude Data for

Pamir Earthquakes

Event 1

Station	Δ	m_b	M_s
ALP	71.6		3.38
ALQ	106.3		-4.16
CHG	29.8		-4.20
CTA	90.0		-3.98
FBK	71.5		-4.42
KOD	28.5	4.27	
KON	44.4		-3.65
LAO	95.0	5.05	-4.94
NAO	44.0	4.39	3.11
POO	20.0	3.97	
TLO	57.9		-3.23
RINGDAL ESTIMATE		4.42	3.19

\- negative sign indicates no signal visible, and upper bound on M_s is computed from background noise

Event 2

Station	Δ	m_b	M_s
ALP	70.9		-3.63
ALQ	105.6		4.26
BUL	72.6	4.57	
CHG	30.3		3.90
CTA	90.4		4.29
FBK	70.7		4.00
KON	43.8		4.57
NAO	43.3	4.23	4.56
NUR	36.6	4.47	
OGD	94.3		4.52
POO	20.8	4.28	-4.42
SHI	19.6	3.82	-4.22
SHL	20.8		3.95
TAB	21.0	4.67	3.63
TLO	57.5		3.62
RINGDAL ESTIMATE		4.34	4.04

Event 3

Station	Δ	m_b	M_s
ALP	71.5		-3.46
ALQ	105.9		4.61
BUL	71.7	4.26	
CHG	30.9		3.41
COL	71.6	4.95	
CTA	91.0		3.86
DAG	52.5	4.37	
KIP	103.4		4.02
KOD	29.1	4.33	
LAO	94.6	5.25	
NAO	43.0	4.13	-4.14
OGD	94.3		4.17
SHL	21.3	3.59	
RINGDAL ESTIMATE		4.41	3.75

Event 4

Station	Δ	m_b	M_s
ALQ	104.6		4.74
ALQ	104.6		4.71
BAG	47.3		4.17
BUL	73.4	4.70	
CTA	90.8	5.15	4.10
DAG	51.3	4.70	
GDH	63.5	5.00	
KON	42.9		4.58
LAO	93.0	5.72	4.44
MAT	49.8		4.33
MAT	49.8	4.54	4.23
NAO	42.4	4.47	4.61
NUR	35.6	3.60	
OGD	93.2		4.49
SDB	78.2	5.22	
SHI	20.0	4.45	4.05
TAB	20.9		3.71
TLO	57.0		4.23
RINGDAL ESTIMATE		4.75	4.34

Event 5

Station	Δ	m_b	M_s
ALP	70.9		-3.53
ALQ	105.7		-4.10
BAG	46.5	5.03	4.23
BUL	72.9	5.16	
CHG	29.8		3.60
CTA	89.8	5.00	-4.37
EIL	33.3		4.22
KIP	102.3		4.28
KON	44.3	4.53	4.35
LAO	94.4	4.59	3.69
MAT	49.7		4.23
MAT	49.7		4.10
MAT	49.7		4.05
NAI	52.9	4.54	4.58
NAO	43.8	4.77	4.07
NUR	36.9	4.47	3.99
OGD	94.7		-3.43
SHI	20.0	4.48	
TAB	21.5		3.43
TLO	58.0		-4.08
TLO	58.0		3.79
RINGDAL ESTIMATE		4.73	3.92

Event 6

Station	Δ	m_b	M_s
ALP	71.0		-3.70
ALQ	105.8		4.58
ALQ	105.8		4.48
BAG	46.5	5.30	4.71
BUL	72.9	5.31	
CHG	29.8		4.45
CHG	29.8	4.35	4.28
CTA	89.8	5.10	4.21
EIL	33.2		4.81
GDH	64.9		4.47
IST	34.0		3.96
KIP	102.3		4.59
KON	44.3	4.23	4.86
KON	44.3		4.74
LAO	94.5	4.74	4.32
MAT	49.7		4.39
MAT	49.7		4.65
MAT	49.7		4.60
NAI	52.8	4.70	4.12
NAO	43.8	4.79	4.65
NUR	36.9	4.47	4.51
OGD	94.7		-3.91
SHI	20.0	4.54	
SNG	40.1		4.05
STU	46.0	4.76	4.35
TAB	21.4		4.03
TLO	58.0		4.33
TLO	58.0		4.20
RINGDAL ESTIMATE		4.75	4.37

Event 7

Station	Δ	m_b	M_s
ALP	70.8		3.57
ALQ	105.6		4.65
ALQ	105.6		4.10
BAG	46.8	5.16	
BUL	72.9	4.65	
CHG	30.1	3.84	
EIL	33.1		3.70
GDH	64.6	5.00	4.44
IST	33.7		3.77
KIP	102.3		-4.69
KON	44.0	4.94	4.90
KON	44.0		4.20
LAO	94.2	5.49	4.07
MAT	49.9		3.91
MAT	49.9		-4.11
MAT	49.9		4.12
NAI	52.8	4.66	
NAO	43.5	5.08	4.30
NUR	36.6	4.80	3.81
OGD	94.4		-4.85
SHI	20.7	4.24	
STU	45.7	4.80	
TAB	21.2	4.67	3.49
TLO	57.7		4.19
TLO	57.7		4.08
RINGDAL ESTIMATE		4.78	4.06

Event 8

Station	Δ	m_b	M_s
ALP	71.0		-3.48
ALQ	105.8		-4.62
ALQ	105.8		4.21
BAG	46.5	5.08	
BUL	72.9	4.74	
CHG	29.8		4.26
CHG	29.8	4.30	3.96
CHG	29.8		3.66
CTA	89.8		4.46
EIL	33.2		4.20
KIP	102.4		4.27
KON	44.3		4.42
LAO	94.5		4.15
MAL	59.8		4.39
MAT	49.8		4.13
MAT	49.8	4.36	4.14
NAO	43.9	4.77	4.59
NUR	36.9	4.46	3.99
OGD	94.8		3.42
SHI	20.0	3.82	-4.24
TAB	21.5	4.90	3.60
TLO	58.0		4.56
TLO	58.0		4.32
RINGDAL ESTIMATE		4.56	4.10

Event 9

Station	Δ	m_b	M_s
ALP	70.9		-2.75
ALQ	105.8		4.44
BAG	46.5	4.87	
BUL	72.9	4.56	
CHG	29.8		-3.57
CTA	89.8		-4.27
EIL	33.3		3.40
KIP	102.3		-3.44
KON	44.3	4.64	3.77
LAO	94.4	4.44	3.67
MAT	49.7		-2.55
MAT	49.7	4.36	3.44
NAO	43.8	4.51	3.88
NUR	36.9	4.46	
OGD	94.7		-3.67
SHI	20.0	3.73	
TLO	58.0		-3.49
TLO	58.0		3.22
RINGDAL ESTIMATE		4.45	3.24

Event 10

Station	Δ	m_b	M_s
BAG	46.6		4.26
BUL	72.8	4.56	
CHG	29.9		3.56
CTA	89.9	4.37	-4.35
DAG	52.5	4.36	
KON	44.2	4.50	4.32
KON	44.2		4.10
LAO	94.4		4.93
MAT	49.8		4.47
MAT	49.8	4.46	4.11
MAT	49.8		4.33
NAO	43.7		4.13
NUR	36.8	4.50	4.11
OGD	94.6		-3.26
SHI	19.9	4.12	3.67
TAB	21.3		3.42
TLO	57.9		-3.54
TLO	57.9		3.52
RINGDAL ESTIMATE		4.41	3.94

Event 11

Station	Δ	m_b	M_s
ALP	70.9		3.65
ALQ	105.8		-4.67
ALQ	105.8		4.94
BAG	46.5		4.16
BUL	72.9	4.56	
CHG	29.8	4.09	4.03
CHG	29.8		3.82
CTA	89.8		4.08
DAG	52.5	4.70	
EIL	33.3		4.01
IST	34.0		3.83
KIP	102.3		4.31
KON	44.2		-5.11
KON	44.2		4.72
LAO	94.4	5.02	-4.43
LEM	55.7		-4.49
MAT	49.7		4.38
MAT	49.7	4.67	4.41
NAI	52.9		4.15
NAO	43.8		4.54
NUR	36.9	4.80	-4.77
PMG	83.3	5.60	
SHI	20.0	4.20	4.29
SNG	40.1		3.57
TLO	58.0		4.11
TLO	58.0		3.88
RINGDAL ESTIMATE		4.70	4.14

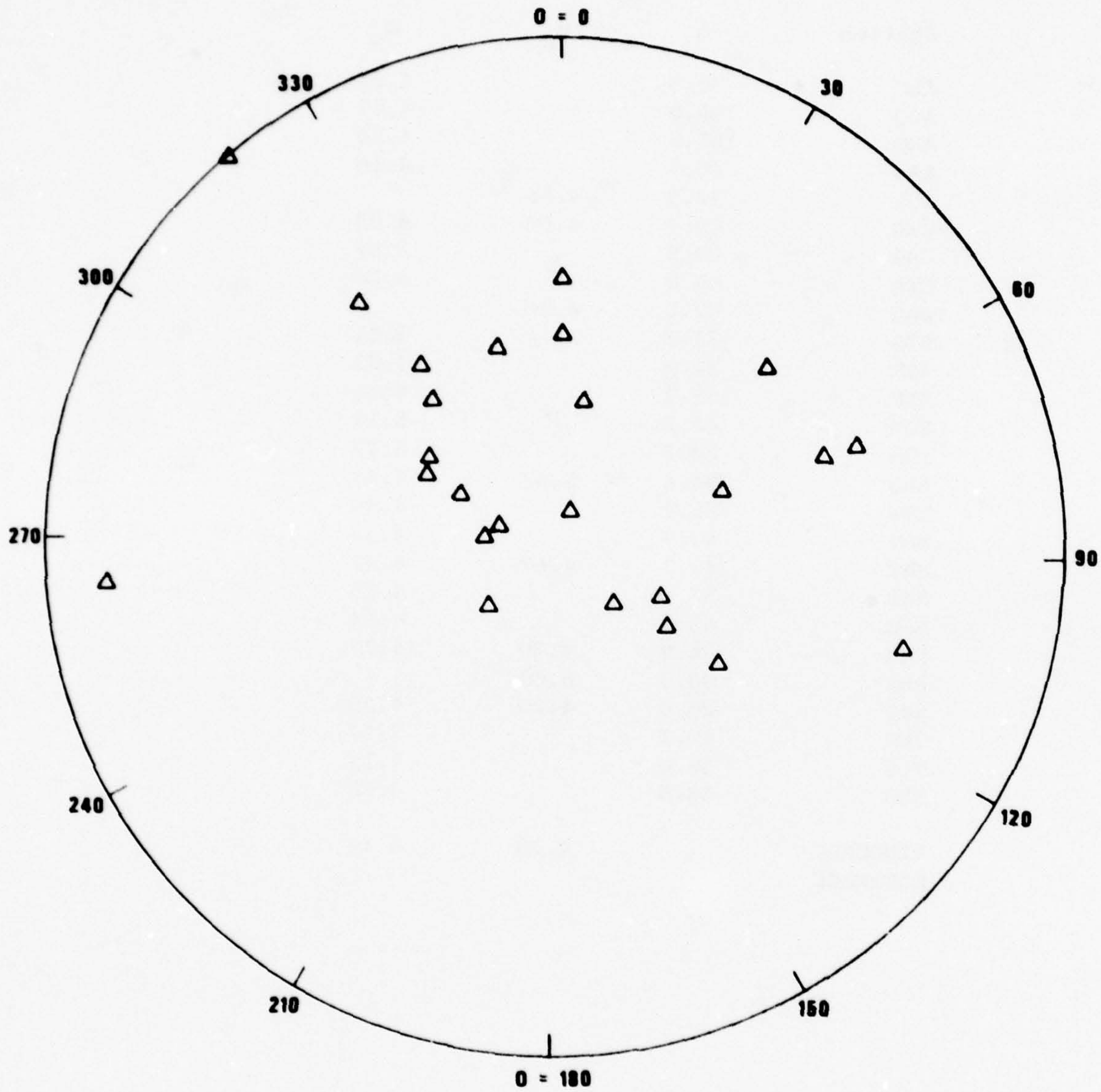

Figure 6. Observed LR amplitudes (T = 20 sec) for Pamir event 6

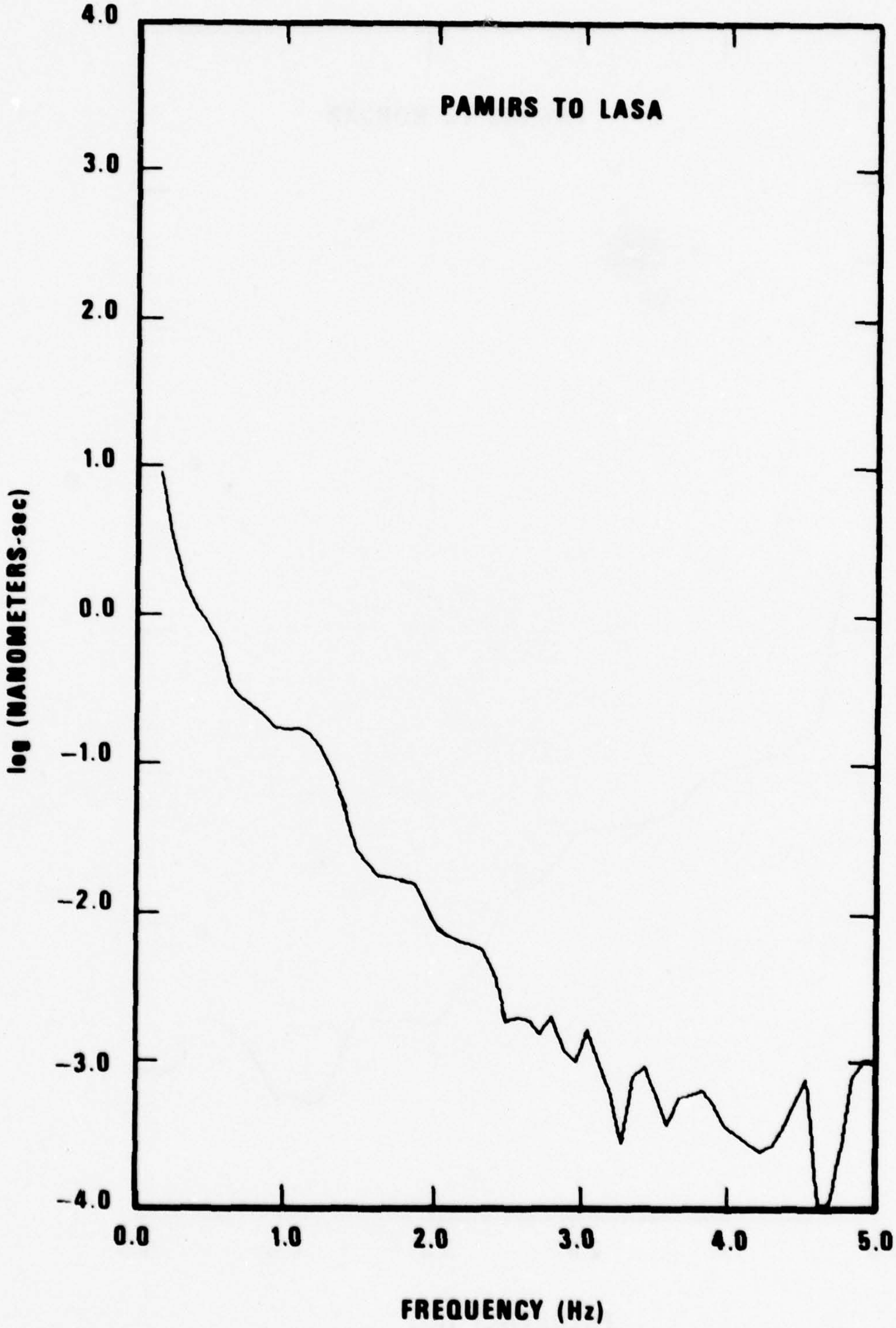

Figure 7. Average of all spectra for the path Pamirs to LASA

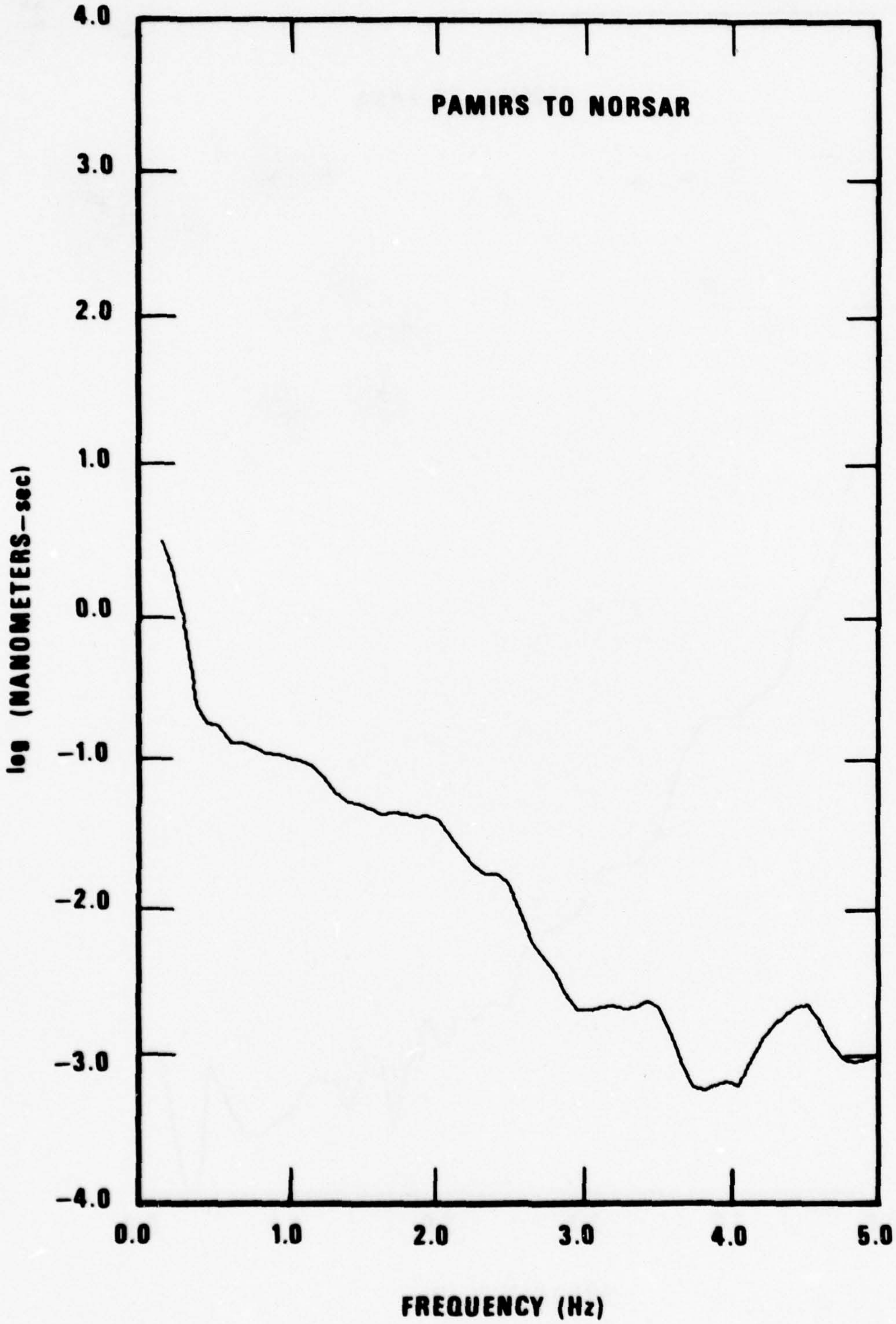

Figure 8. Average of all spectra for the path Pamirs to NORSAR

where $A(f)$ is the observed spectrum (corrected for seismograph response), S is the source spectrum scale constant, and f is frequency in Hz. Then after taking the natural log of this equation

$$\ln[A(f)] + 2 \cdot \ln(f) - \ln(S) = -\pi f t^*$$

or

$$\ln(A) + 2 \cdot \ln(f) = -\pi t^* f + \ln(S)$$

If we plot $\ln(A) + 2 \cdot \ln(f)$ versus frequency for each path, as shown in Figures 9 and 11, the slope of the graph is $-\pi t^*$. We calculated the slope in the frequency range 1.0 to 2.5 Hz, where the signal-to-noise ratio was highest, and presumably beyond the corner frequency so that the high-frequency asymptotic slope of f^{-2} characterizes the source spectrum. Similarly, the equation for the source spectra with an f^{-3} falloff is

$$\ln(A) + 3 \cdot \ln(f) = -\pi t^* f + \ln(S)$$

If we plot the left-hand side of this relation versus frequency for each path, as shown in Figures 10 and 12, the slope of the graph is again $-\pi t^*$; but t^* now is based on an assumed f^{-3} source spectrum. The t^* values for an f^{-2} source model are $.53 \pm .09$ for the Pamir to LASA path and $.00 \pm .05$ for the Pamir to NORSAR path. The t^* values for an f^{-3} source model are $.34 \pm .08$ for the Pamir to LASA path and $-.18 \pm .06$ for the Pamir to NORSAR path. Since a negative t^* path is unrealistic, the f^{-3} t^* value for the Pamir to NORSAR path is set equal to zero. The Pamir to NORSAR path has less attenuation as expected since the path is mostly through continental shield areas. Values of t^* for the Kazakh explosions for f^{-2} source models were also calculated. These t^* values are $.16 \pm .10$ for the East Kazakh (events 1 through 4 and 9 and 10) to LASA path, $.05 \pm .08$ for the East Kazakh to NORSAR path, $.29 \pm .13$ for the West Kazakh (events 5 through 8) to LASA path, and $.19 \pm .04$ for the West Kazakh to NORSAR path. As expected the t^* values for the paths to NORSAR are lower than the values for the paths to LASA since the paths to NORSAR are through continental shield areas while those to LASA pass under tectonically active provinces.

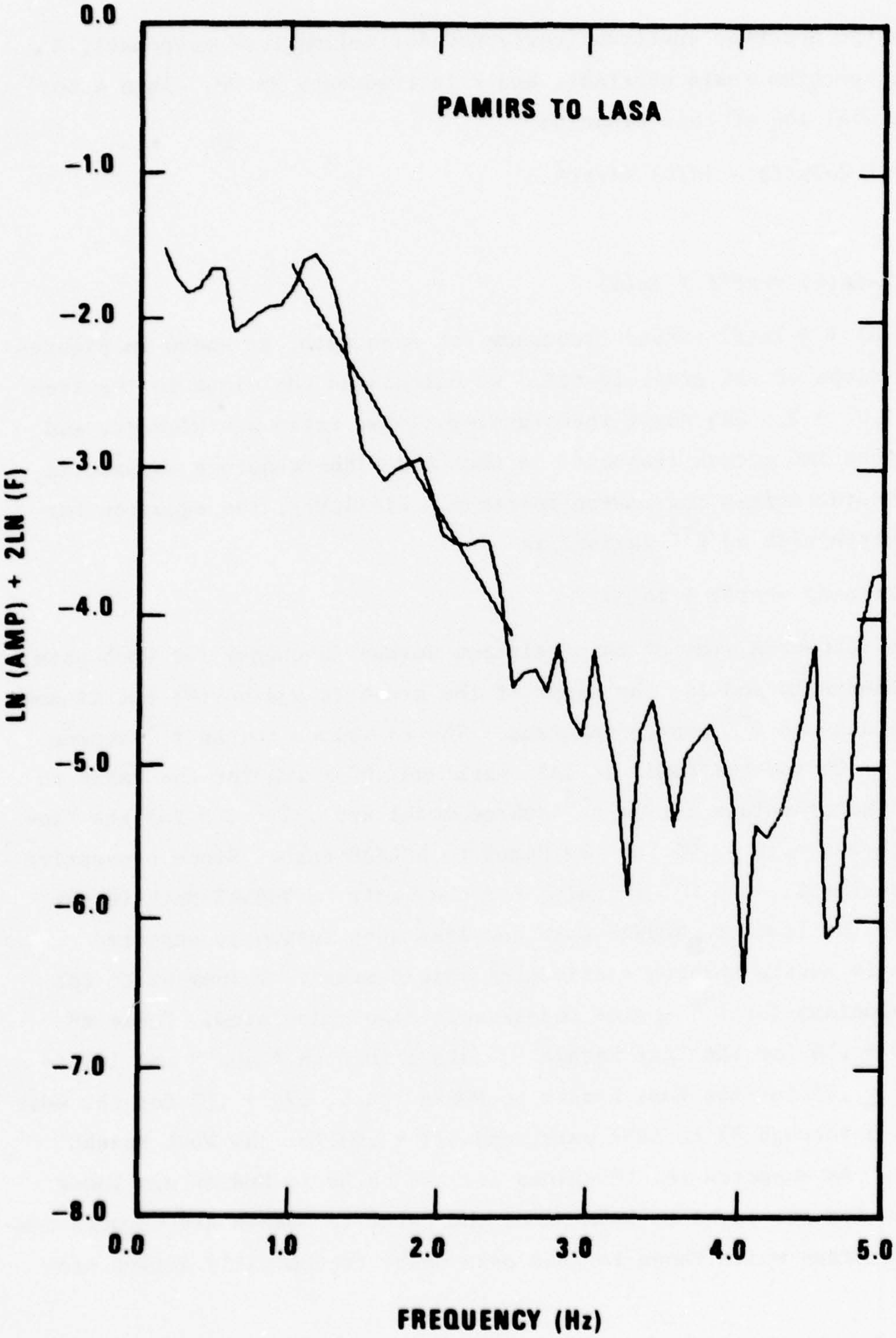

Figure 9. Ln(A) + 2·ln(f) versus frequency for the path Pamirs to LASA

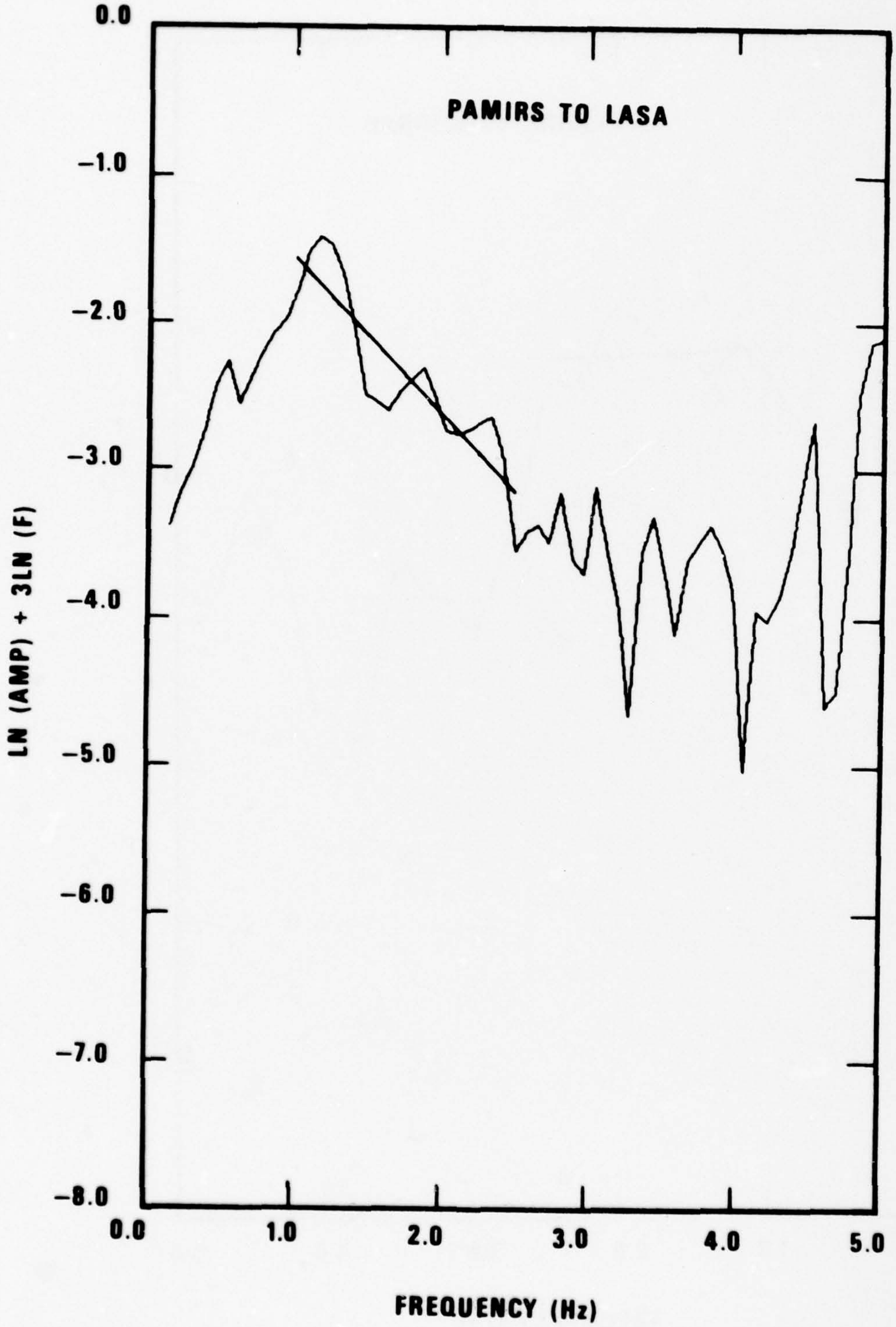

Figure 10. Ln(A) + 3·ln(f) versus frequency for the path Pamirs to LASA

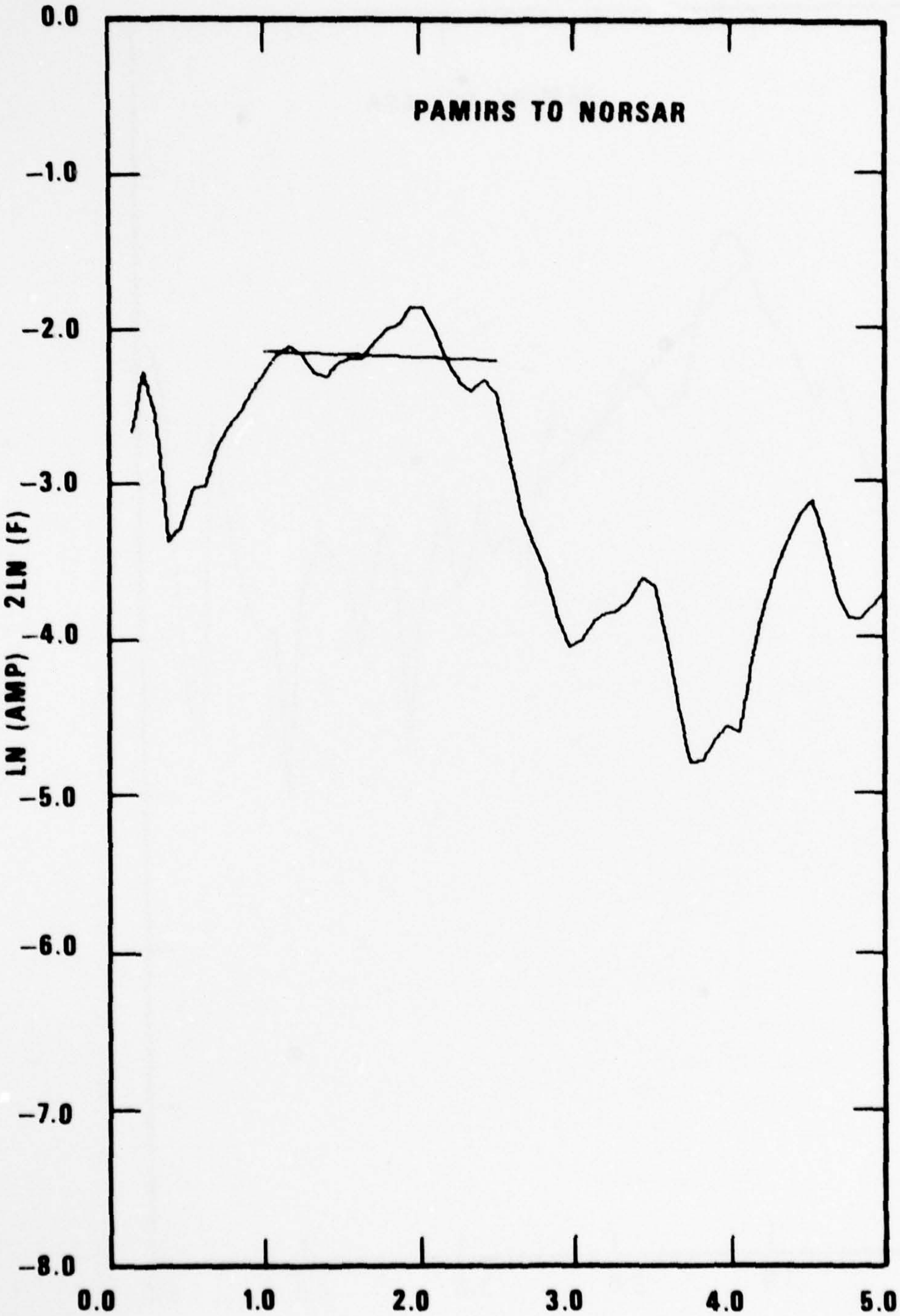

Figure 11. Ln(A) + 2·ln(f) versus frequency for the path Pamirs to NORSAR

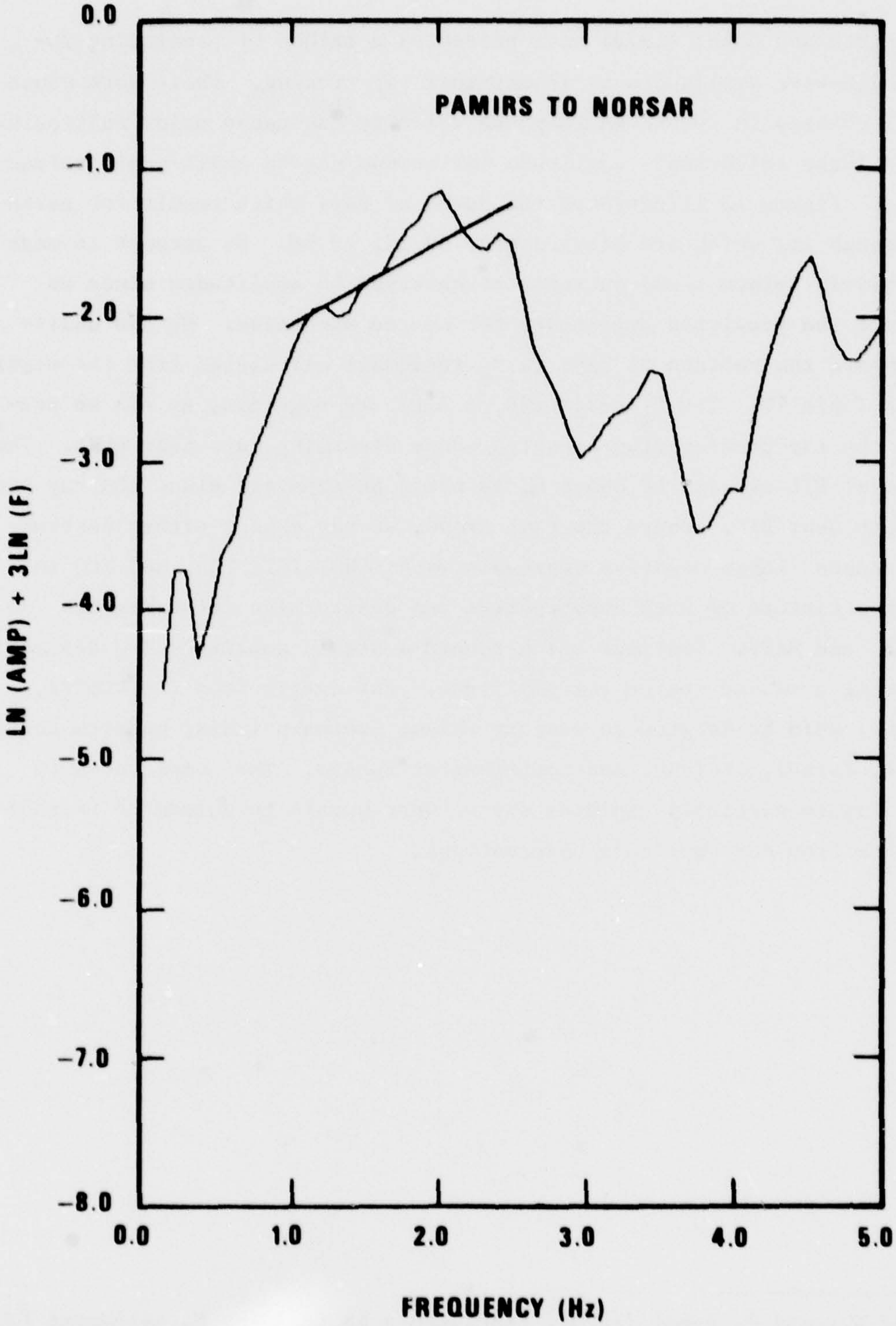

Figure 12. Ln(A) + 3·ln(f) versus frequency for the path Pamirs to NORSAR

Von Seggern and Sobel (1975) have presented a method of predicting 20-second Rayleigh-wave amplitudes by geometrical ray tracing. Their work shows that lateral changes in 20-second LR-phase velocity can cause major multipathing and also large teleseismic amplitude variations due to small-scale refraction effects. Figure 13 illustrates the paths of rays which result for earthquakes 5 through 11, which are grouped near 39.3N, 73.9E. No attempt is made to quantitatively relate these patterns to observed LR amplitudes since we cannot correct the predicted amplitudes for source mechanism. We can qualitatively compare the pattern of rays to M_s residuals calculated from the magnitude data in Table IV. The M_s residuals at ALPA are negative, as can be predicted from the ray tracing diagram which shows diverging rays near ALPA. The M_s residuals at EIL average to about 0, as would be expected since the ray pattern is smooth near EIL. Where the rays cross, we can expect either destructive interference (large negative residuals as at CHG, IST, TAB, and TLQ in Table IV) or a mixture of both constructive and destructive interferences (as at CTA, LASA, and MAT). Stations which record a stable amplitude are desirable for calibrating a source region for amplitude. For events from the Pamirs, such stations could be located in eastern China, southern India, western Saudi Arabia, Iraq, Israel, Finland, and northcentral Russia. The complicated LR ray-tracing figure partially explains why we were unable to determine LR radiation patterns from our amplitude observations.

---

von Seggern, D., and P. Sobel (1975), Experiments in refining M_s estimates for seismic events, SDAC Reprot No. TR-75-17, Teledyne Geotech, Alexandria, Virginia.

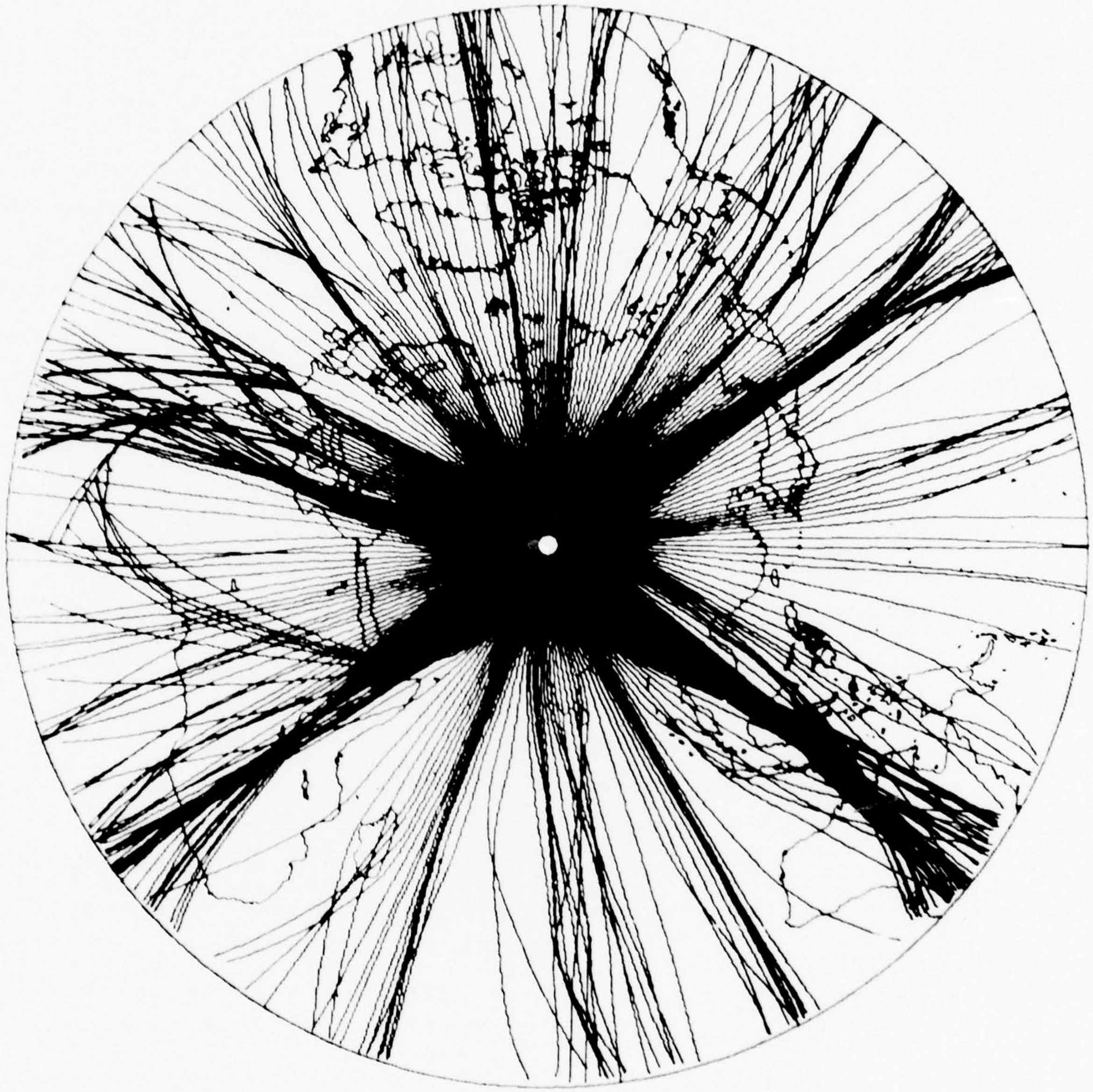

Figure 13. Predicted LR raypaths (T = 20 sec) for events 5 through 11 (39.3N, 73.9E)

DISCRIMINATION ASPECTS

M_s-m_b

In this and the following sections we apply several common discriminants between earthquakes and explosions to the Pamir earthquakes and Kazakh explosions. We had chosen those Pamir events which, during preliminary screening, were of low M_s for their m_b. Then we independently determined average M_s and m_b values for the Pamir events in Table II using WWSSN stations, HGLP stations and the ALPA, LASA, and NORSAR arrays. The data used in the average estimates are listed in Table IV. Negative values in the table indicate noise measurements which were used as upper bounds for the signal amplitudes. Magnitudes were computed according to the formulas

$$m_b = \log(A/T) + B(\Delta)$$
$$M_s = \log(A/T) + 1.66 \log\Delta + 0.3$$

where A = one-half the peak-to-peak maximum recorded amplitude reduced to mμ ground displacement,

T = period in seconds (restricted to 17 to 23 sec for M_s calculations),

Δ = epicentral distance in degrees,

B(Δ) = Gutenberg-Richter correction term for surface-focus P waves.

We also independently determined M_s for the Kazakh explosions in Table III using the NORSAR array and HGLP stations. The data used in the average estimates for explosion M_s are listed in Table V, and explosion m_b values are from NEIS list. We have throughout used a method of magnitude estimation proposed by Ringdal (1976), in which the magnitudes at the individual stations are assumed to follow a gaussian distribution. Among this distribution, some magnitudes will fall below the noise level, and Ringdal's method then substitutes a noise measurement at those stations which do not detect and computes the maximum likelihood estimate of magnitude based on measured signals and noise. The effect of this procedure is to more accurately define the magnitude of events not widely recorded. Based on this method, average magnitude values for small events, where many of the readings are noise levels, are lower than what would

---

Ringdal, F. (1976), Maximum-likelihood estimate of event magnitude, Bull. Seism. Soc. Am., 66, 789.

Table V

Magnitude Data for Kazakh Explosions

Event 1

Station	Δ	M_s
CHG	35.1	3.23
Ringdal Estimate		3.23

Event 2

Station	Δ	M_s
CHG	35.2	-3.47
EIL	38.1	-4.45
KON	38.9	3.59
NAO	38.0	3.49
Ringdal Estimate		3.47

Event 3

Station	Δ	M_s
CHG	35.2	3.48
EIL	38.1	3.71
KON	38.9	3.59
NAO	38.0	3.96
Ringdal Estimate		3.68

Event 4

Station	Δ	M_s
KON	39.1	-3.73
Ringdal Estimate		-3.73

Event 5

Station	Δ	M_s
CHG	42.8	-3.44
KON	30.7	2.86
Ringdal Estimate		2.86

Event 6

Station	Δ	M_s
CHG	35.8	-3.83
KON	38.4	3.64
MAT	53.3	-3.85
Ringdal Estimate		3.60

Event 7

Station	Δ	M_s
KON	36.6	3.31
MAT	52.1	-4.08
Ringdal Estimate		3.31

Event 8

Station	Δ	M_s
KON	26.0	3.54
Ringdal Estimate		3.54

Event 10

Station	Δ	M_s
NAO	37.9	-3.1
Ringdal Estimate		-3.1

Event 9

Station	Δ	M_s
NAO	38.1	-2.61
Ringdal Estimate		-2.61

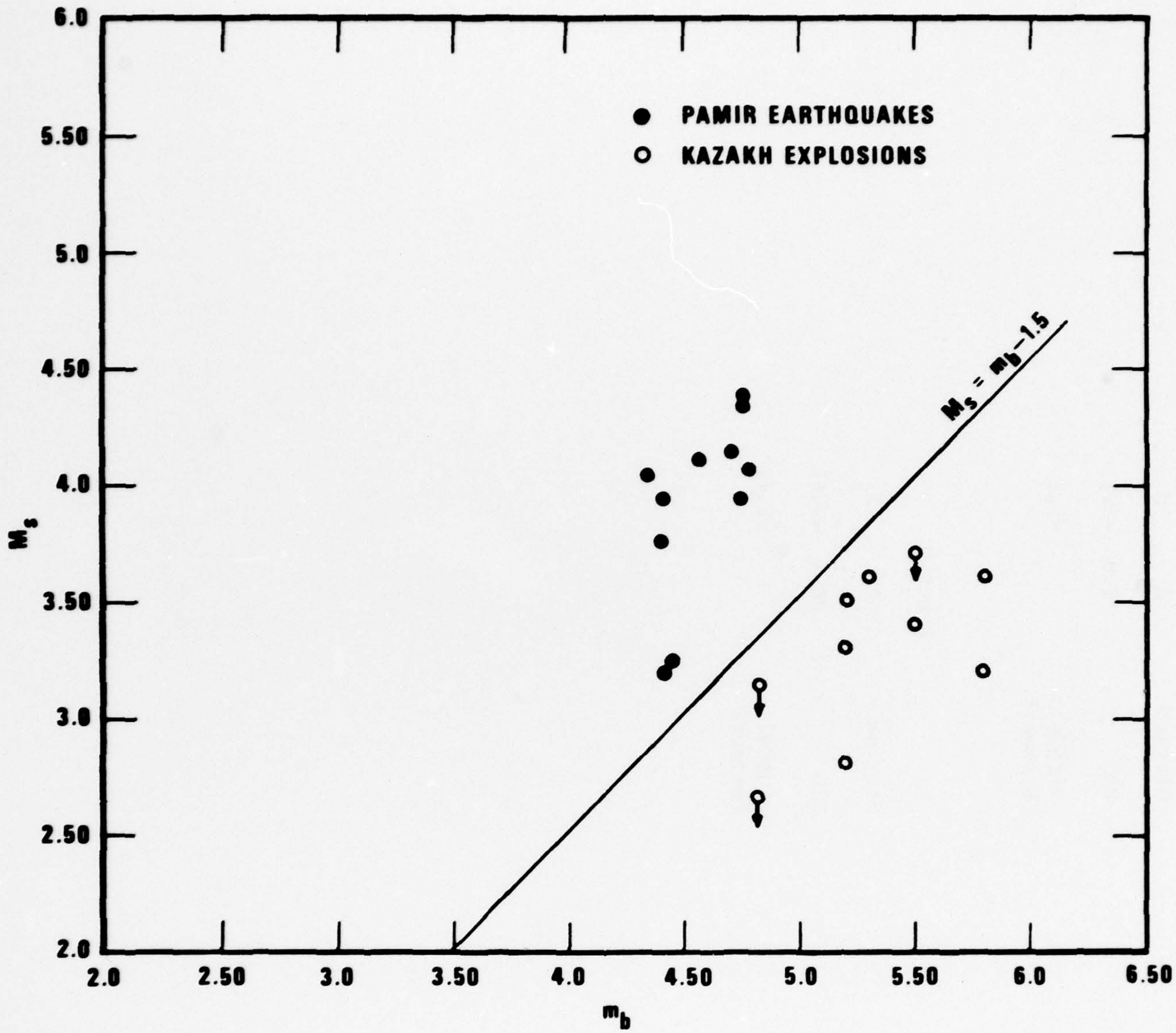

Figure 14. M_s versus m_b for Pamir earthquakes and Kazakh explosions

result if only measured signal amplitudes were used. The magnitude averages for the Pamir earthquakes and Kazakh explosions are shown in Figure 14. Arrows indicate M_s values based solely on noise measurements. In these cases the maximum M_s value was used as the M_s value. The line $M_s = m_b - 1.5$ (arbitrarily drawn here) clearly separates the Pamir earthquakes from the Kazakh explosion population. This line would also separate the suite of Asian events studied by Dahlman et al. (1974). The Kazakh explosions are located in two test areas approximately 10 to 15 degrees northwest and northeast of the Pamir earthquakes.

Corner Frequency

Figure 15 is a plot of $|\Omega_o|$ versus corner frequency for the Pamir earthquakes and Kazakh explosions recorded at LASA and NORSAR. No long-period P phases were recorded at the long-period arrays due to the small magnitudes of the events, so the values of $|\Omega_o|$ were estimated from the spectral data of the short-period vertical component. Hanks and Thatcher (1972) have shown that for a given long-period level Aleutian explosions have a higher corner frequency than Aleutian earthquakes. The physical basis of this discriminant is the smaller source time dimension of the explosion for a given long-period level. However, Figure 15 shows no separation between the Pamir earthquakes and the Kazakh explosions. Furthermore, there is only a slight trend toward higher corner frequencies for lower $|\Omega_o|$ for both the explosions and the earthquakes.

One possible reason that no separation was observed is that this study used only short-period P recordings, whereas Hanks and Thatcher used long-period body wave recordings. Another possible explanation is that due to the low magnitudes of the events studied here, a clear asymptotic value of $|\Omega_o|$ was not possible in most cases. Finally, the lack of separation could be due to characteristics of the sources examined in this study which were not present

---

Dahlman, O., H. Israelson, A. Austegard, and G. Hornstrom (1974), Definition and identification of seismic events in the USSR, Bull. Seism. Soc. Am., 64, 607.

Hanks, T, and W. Thatcher (1972), A graphical representation of seismic source parameters, J. Geophys. Res., 77, 4393.

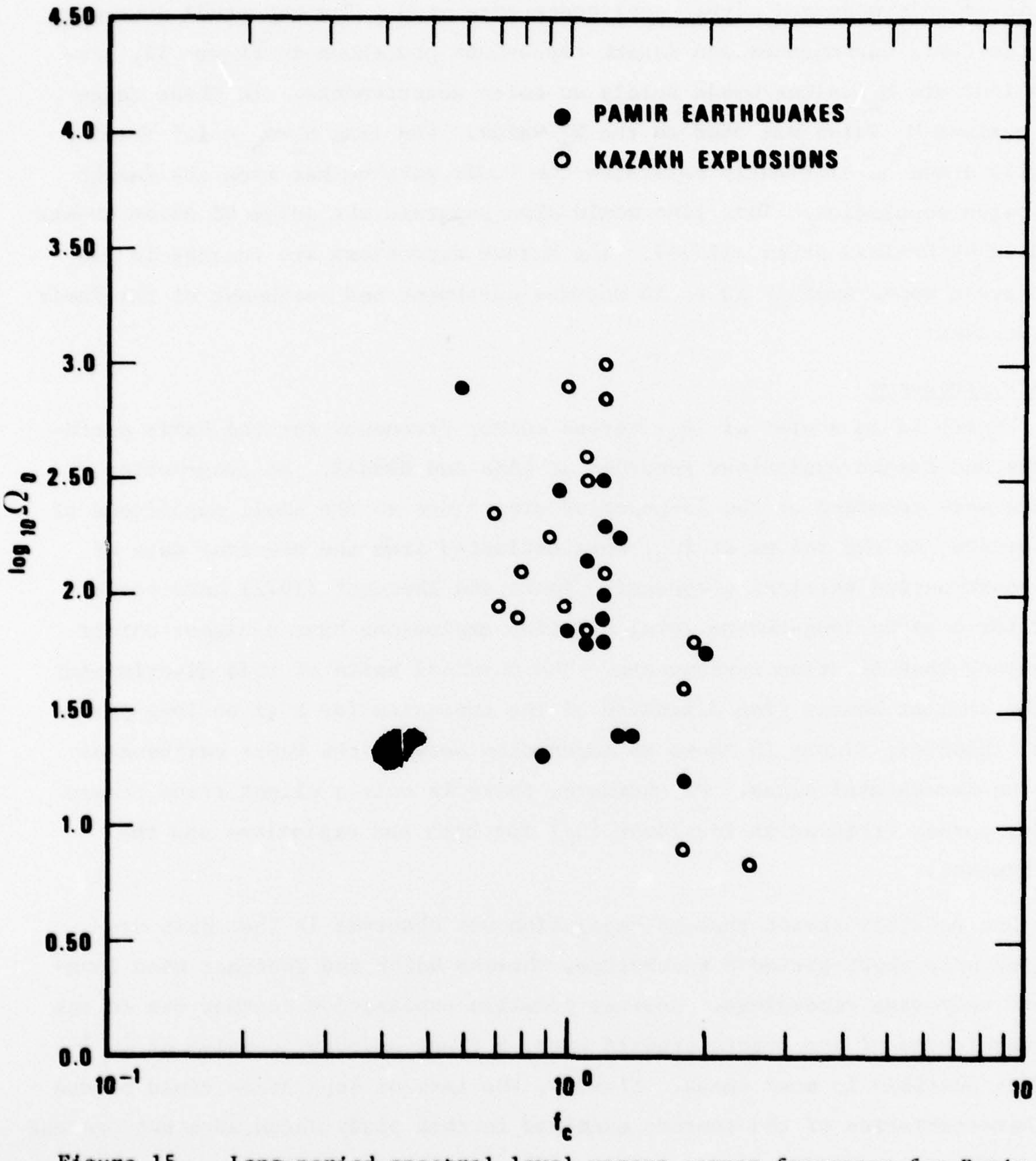

Figure 15. Long-period spectral level versus corner frequency for Pamir earthquakes and Kazakh explosions from LASA and NORSAR P recordings

in the Aleutian events studied by Hanks and Thatcher. For example, the source material in the Aleutians was lava and bedded tuffs whereas the source material for the Kazakh explosions was presumed to be granite.

Long-Period Body-Wave Excitation

There were too few long-period P observations to determine average event ratios of these quantities to long-period LR ground displacement. All of the long-period P observations were close to the noise level, as would be expected for these small magnitude events. No clear long-period S waves were observed on the recordings analyzed for the Pamir earthquakes.

Depth of Focus

All of the Pamir events studied here, except event 10, had apparent pP phases recorded at either LASA or NORSAR or both arrays. No LASA or NORSAR short-period data was available for event 10; however, pP for event 10 was observed at a few of the WWSSN stations. The pP phases recorded at the WWSSN stations agreed with the depths determined at LASA and NORSAR for all cases. Thus many low M_s-m_b events in this region could be identified as earthquakes on the basis of pP observations. pP was, of course, not identified for the explosions and does not, therefore, function as a positive discriminant. Also, for crustal-depth events there is little pP moveout, and thus positive identification of this phase is not possible when the observing stations are in a limited epicentral range.

Complexities

We have computed the "complexity" parameter as seen as LASA and NORSAR for the Pamir earthquakes and Kazakh explosions in the manner given by Lambert et al. (1969). Figure 16 shows the complexity values versus m_b. LASA beams for the Pamir events show apparent pP signals for 4 of the 5 cases where complexity was determined. NORSAR beams show apparent pP signals for 5 of the 8 cases where complexity was determined. We believe that the lack of a clear pP signal in the other cases was due to noisy data or to a pP signal that could not be visually separated from the P coda. Complexity numbers were not calculated for some cases because of the low signal-to-noise ratio, which would have made those complexity numbers doubtful. The complexity numbers for the Kazakh ex-

---

Lambert, D., D. von Seggern, S. Alexander, and G. Galat (1969), The LONGSHOT Experiment, Volume II. Comprehensive Analysis, SDL Report No. 234, Teledyne Geotech, Alexandria, Virginia.

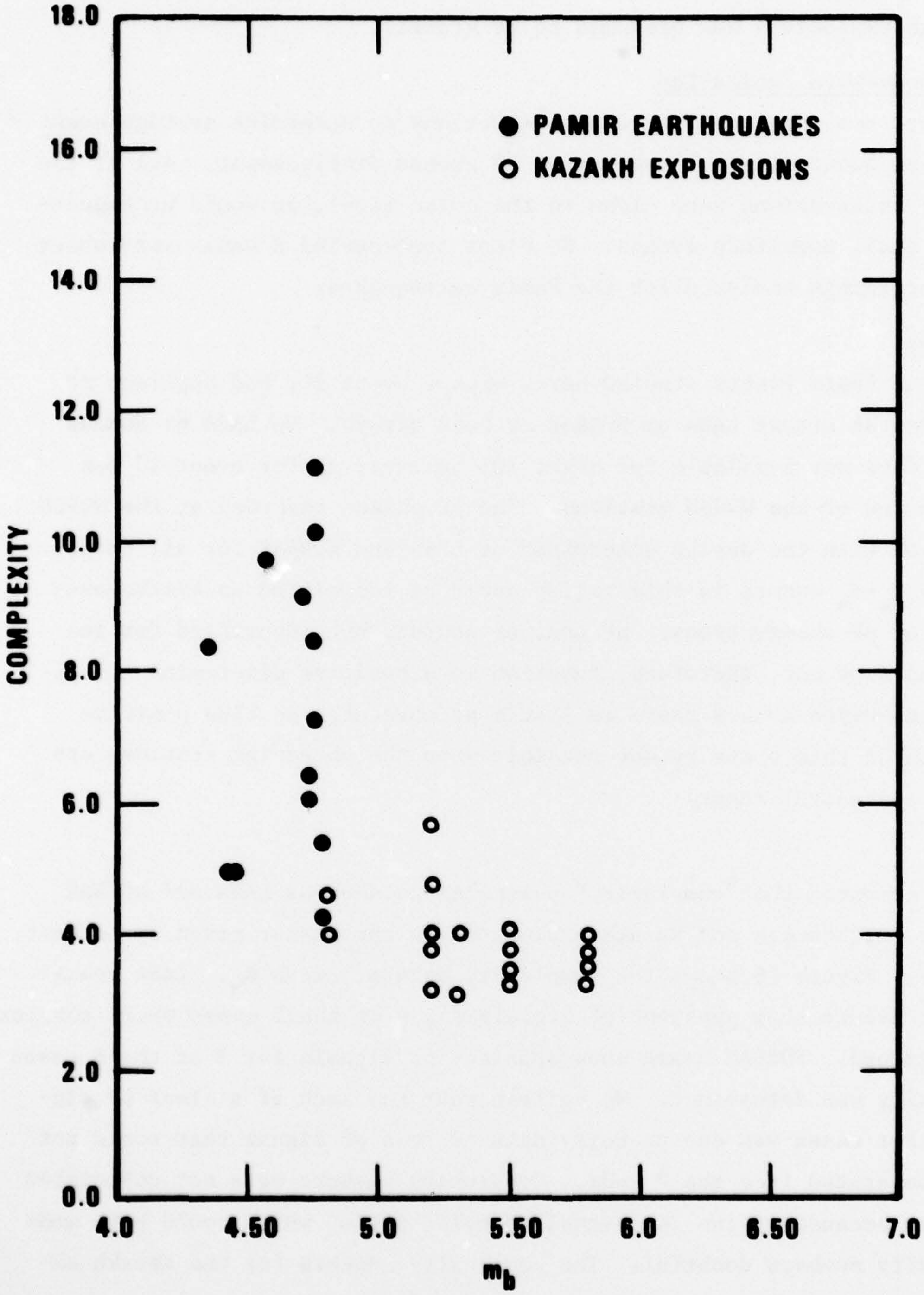

Figure 16. Complexity versus m_b for Pamir earthquakes and Kazakh explosions from LASA and NORSAR P recordings

plosions were low (3.08-5.66) as would be expected for an explosion. The complexity numbers for the Pamir events were generally higher (4.24-11.09), but overlap the numbers for the Kazakh explosions. Due to the relatively low attenuation of the Pamir earthquake signals at LASA and NORSAR, we cannot ascribe the higher complexity of the earthquakes to attenuation of the initial P as suggested by Douglas et al. (1973); therefore the additional earthquake coda energy must be related to source mechanism and crustal effects.

Spectral Ratios

Spectral ratios have been calculated at LASA and NORSAR according to a form suggested by Lacoss (1969):

$$R = \int_{1.55}^{1.95} A(f)df \Big/ \int_{.45}^{.85} A(f)df$$

where sums of the equivalent terms of the discrete Fourier transform have replaced the amplitude spectrum integrals over A(f). These ratios are plotted against m_b in Figure 17 for the Pamir earthquakes and Kazakh explosions for the case $t^* = 0$, that is, using the uncorrected spectra. The spectral ratios for the same P recordings are plotted in Figure 18 with t^* values for ω^{-2} source models for earthquakes and explosions and ω^{-3} source models for earthquakes. Bars connect the cases where there are two different t^* values for the two source models. The amplitudes of the P spectra were greater than the amplitudes of the noise spectra in the frequency range 0.4 to 2.5 Hz for all of the LASA and NORSAR beams. For many cases the P spectra were greater than the noise spectra in the range 0.5 to 5.0 Hz. NORSAR signal beams (C3 subarray) possessed more high frequencies and therefore generally had higher spectral ratios than the LASA beams (A0 subarray), in accord with our previous t^* estimates for the two paths. The spectral ratio did not depend on m_b, M_s, or depth. In general, the Kazakh explosions show larger spectral ratios than the Pamir earthquakes, but the explosion and earthquake populations cannot be said to separate.

Douglas, A., P. Marshall, P. Gibbs, J. Young, and C. Blamey (1973), P signal complexity reexamined, Geophys, J., 33, 195.

Lacoss, R. (1969), A large-population LASA discrimination experiment, Technical Note 1969-24, Lincoln Laboratory, Lexington, Massachusetts.

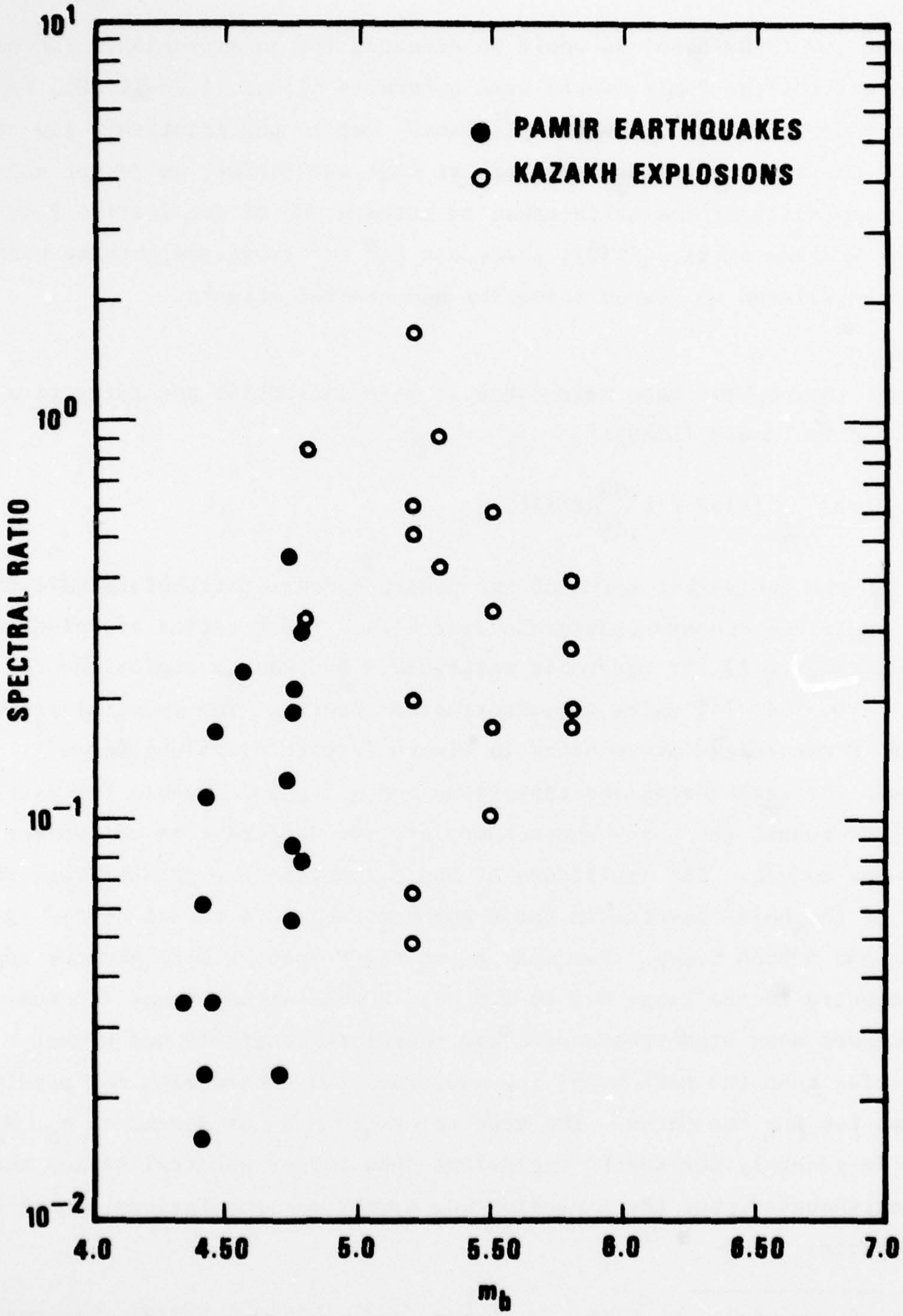

Figure 17. Short-period P spectral ratio versus m_b for Pamir earthquakes and Kazakh explosions recorded at LASA and NORSAR for $t^* = 0$

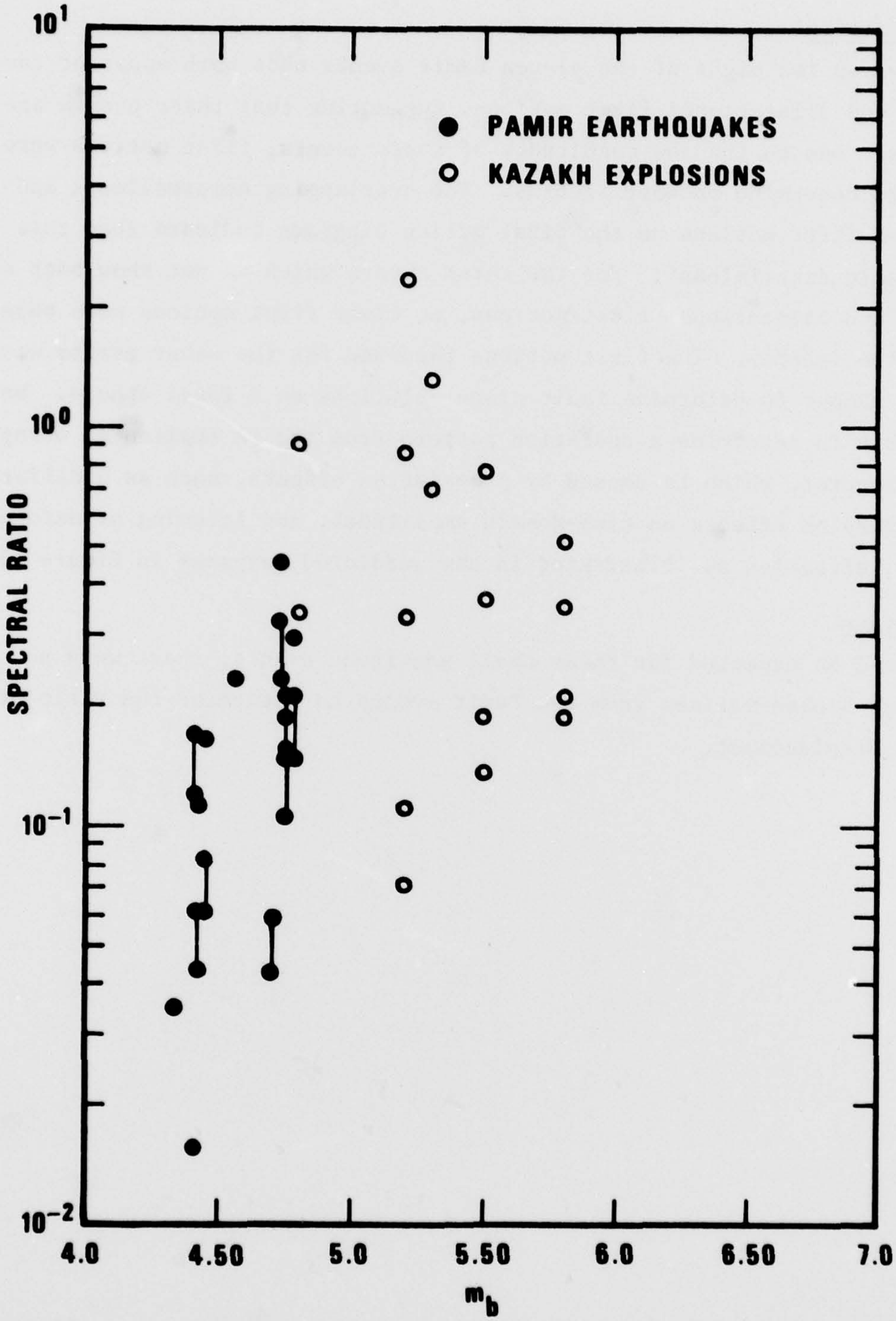

Figure 18. Short-period P spectral ratio versus m_b for Pamir earthquakes and Kazakh explosions recorded at LASA and NORSAR. The t* values are for ω^{-2} source models for earthquakes and explosions and ω^{-3} source models for earthquakes

Radiation Pattern

Body waves for eight of the eleven Pamir events show both apparent compressional and dilatational first motions, suggesting that these events are earthquakes. Due to the low magnitudes of these events, first motions were difficult to determine on most records. The overlapping compressional and dilatational first motions on the first motion diagrams indicate that this is not a reliable discriminant. For the three events which do not show both compressional and dilatational first motions, no clear first motions were observed on any of the records. The first motions recorded for the other events were too few in number to determine fault plane solutions on a focal sphere. We were not able to determine a radiation pattern from the LR amplitudes owing to the large scatter, which is caused by propagation effects, such as Q differences, dispersion effects on time-domain amplitudes, and focusing or defocusing due to refraction as illustrated in the predicted raypaths in Figure 13.

S/P Excitation

As would be expected for these small magnitude events, there were no short-period S observations from the Pamir events to determine the ratio of S/P ground displacement.

SUMMARY

Eleven events with low reported M_s for their m_b from the Northern Pamirs and ten Kazakh explosions were examined in a seismic discrimination context. All the Pamir events lie close to major faults observed in satellite photographs. It was impossible on the basis of first motions to determine fault plane solutions due to the small magnitudes of the events. We were also unable to determine a radiation pattern from the LR amplitudes, probably due to varying propagation effects. The following characteristics of the Pamir events indicate that all the events are earthquakes:

- All the presumed earthquakes had consistent pP phases recorded at LASA, NORSAR, or some of the WWSSN stations. Although little moveout for pP can be detected for shallow earthquakes, the clarity and size of the phase was sufficient in most cases to identify it with some confidence.
- All the Pamir events studied here fall above the line $M_s = m_b - 1.5$. The Kazakh explosions clearly lie below the line $M_s = m_b - 1.5$.

There are other areas in Asia, notably near 30°N, 95°E, where earthquakes do not clearly separate from explosions in Asia on an M_s-m_b plot. Also shot arrays could be used to raise the M_s of an explosion by about 0.3 M_s units or more without raising m_b, placing it close to the earthquake population studied here.

Complexity and spectral ratio were not useful discriminants in this data set. The low magnitudes of the earthquakes studied here (m_b from 4.3 to 4.8 and M_s from 3.2 to 4.4) made clear discrimination difficult with the available data and probably represents nearly the lowest threshold of discrimination for the stations and area studied in this report. The installation of high-quality SRO stations in Asia will permit the examination of lower-magnitude events with multistation short-period data.

REFERENCES

Aliev, S., N. Beliaevsky, E. Butovskaya, B. Volvovsky, I. Volvovsky, G. Krasnopevtseva, V. Pak, M. Polshkov, V. Rubailo, V. Sallogub, B. Tal-Virsky, F. Tregub, I. Khamrabayev, and G. Kharechko (1976), The seismic experiment in the Northern Pamirs, in Geodynamics: Progress and Prospects, ed. C. Drake, American Geophysical Union.

Archambeau, C., E. Flinn, and D. Lambert (1969), Fine structure of the upper mantle, J. Geophys, Res, 74, 5825.

Ben-Menahem, A., S. Smith, and T. Teng (1965), A procedure for source studies from spectrum of long-period seismic body waves, Bull. Seism. Soc. Am., 55, 203.

Bungum, H., and D. Tjostheim, (1976), Discrimination between Eurasian earthquakes and underground explosions using the m_b:M_s method and short-period autoregressive parameters, Geophys. J., 45, 371.

Dahlman, O., H. Israelson, A. Austegard, and G. Hornstrom (1974), Definition and identification of seismic events in the USSR, Bull. Seism. Soc. Am., 64, 607.

Douglas, A., P. Marshall, P. Gibbs, J. Young, and C. Flamey (1973), P signal complexity reexamined, Geophys, J., 33, 195.

Hanks, T., and W. Thatcher (1972), A graphical representation of seismic source parameters, J. Geophys. Res., 77, 4393.

Keilis-Borok, V. I. (1960), Investigation of the Mechanism of Earthquakes, English translation, American Geophysical Union, Washington, D.C.

Kosminskaya, I., G. Mikhota, and Y. Tulina (1958), Crustal structure of the Pamir-Alai zone from seismic depth-sounding data, Izvestiya, Geophysics Series, 673.

Lacoss, R. (1969), A large-population LASA discrimination experiment, Technical Note 1969-24, Lincoln Laboratory, Lexington, Massachusetts.

Lambert, D., D. von Seggern, S. Alexander, and G. Galat (1969), The LONGSHOT Experiment, Volume II. Comprehensive Analysis, SDL Report No. 234, Teledyne Geotech, Alexandria, Virginia.

Molnar, P., T. Fitch, and F. Wu (1973), Fault plane solutions of shallow earthquakes and contemporary tectonics in Asia, Earth and Planetary Science Letters, 19, 101.

Molnar, P., and P. Tapponnier (1975), Cenozoic tectonics of Asia: effects of a continental collison, Science, 189, 419.

REFERENCES (Continued)

Ringdal, F. (1976), Maximum-likelihood estimate of event magnitude, Bull. Seism. Soc. Am., 66, 789.

Ritsema, A. (1966), The fault-plane solutions of earthquakes of the Hindu Kush centre, Tectonophysics, 3, 147.

Semyenov, A. N. (1969), Variations in the travel time of transverse and longitudinal waves before violent earthquakes, Izvestiya, Phys. Solid Earth, No. 4, 245.

Shirokova, E. (1967), General features in the orientation of principal stresses in earthquake foci in the Mediterranean-Asian seismic belt, Izvestiya, Phys. Solid Earth, No. 12, 12.

Vinnik, L. P., and A. Godzikoskaya (1973), Lateral variations of the absorption by the upper mantle beneath Asia, Izvestiya, Earth Physics, No. 1, 3.

Vinnik, L. P., and A. A. Lukk (1974), Lateral inhomogeneities of the upper mantle under the Pamir and Hindu-Kush, Izvestiva, Earth Physics, No. 1, 9.

von Seggern, D., and P. Sobel (1975), Experiments in refining M_s estimates for seismic events, SDAC Report No. TR-75-17, Teledyne Geotech, Alexandria, Virginia.